X-621-72-234

PREPRINT

NASA TM X- 65960

A NUMERICAL STUDY OF A THREE DIMENSIONAL SPHERICAL THERMOSPHERIC DENSITY AND WIND MODEL

H. VOLLAND

H. G. MAYR

JUNE 1972

GSFC

GODDARD SPACE FLIGHT CENTER

GREENBELT, MARYLAND

X-621-72-234

A NUMERICAL STUDY OF A THREEDIMENSIONAL SPHERICAL THERMOSPHERIC DENSITY AND WIND MODEL

by

H. Volland
Astronomical Institutes
University of Bonn
Bonn, Germany

and

H. G. Mayr
Goddard Space Flight Center
Greenbelt, Md. USA

June 1972

Goddard Space Flight Center
Greenbelt, Maryland

CONTENTS

	Page
ABSTRACT	vii
1. INTRODUCTION	1
2. BASIC EQUATIONS	2
3. DEVELOPMENT IN TERMS OF TIDAL MODES	6
4. THE VERTICAL STRUCTURE FUNCTION	8
5. THE DETERMINATION OF THE EIGENFUNCTIONS	11
6. MODE COUPLING	16
7. THE FUNDAMENTAL SYMMETRIC DIURNAL TIDAL MODE (1,1,1)	18
8. THE FUNDAMENTAL SYMMETRIC SEMI-DIURNAL TIDAL MODE (2,2,2)	30
CONCLUSION	35
REFERENCES	39

ILLUSTRATIONS

Figure		Page
1	Height profiles of mean temperature T_0, mean velocity of sound c_0, mean collision number $\nu_{0,0}$ and effective collision number ν_{eff} used in the model calculations	18
2	Solar EUV heat input Q_i versus altitude used in the model calculations	20
3	Magnitude (Fig. 3a) and phase (Fig. 3b) of the density coefficient $\rho^1_{1,1}/\rho_0$ of the diurnal (1,1,1)-mode versus altitude generated by solar EUV heat input Q_{III} ("EUV"), by the electric field of the Sq current ("EF") and by a heat source within the lower	

ILLUSTRATIONS–(continued)

Figure		Page
3 (cont)	atmosphere ("TW"). The dashed lines give the sum of the three contributions. The thin solid lines have been calculated adopting heat sources Q_I and Q_{II} from Fig. 2	21
4	Magnitude (Fig. 4a) and phase (Fig. 4b) of the meridional wind coefficient $u^1_{1,1}/c_0$ of the diurnal (1,1,1)-mode versus altitude generated by the solar EUV heat input Q_{III} ("EUV") by the electric field of the Sq current ("EF") and by a heat source within the lower atmosphere ("TW"). The dashed lines give the sum of the three contributions	24
5	Magnitudes (Fig. 5a) and phases (Fig. 5b) of the coefficients of pressure $p^1_{1,1}/p_0$, temperature $T^1_{1,1}/T_0$, zonal wind $v^1_{1,1}/c_0$ and vertical wind $w^1_{1,1}/c_0$ of the diurnal (1,1,1)-mode versus altitude generated by the sum of the three wave generators considered	25
6	Height functions determining the latitude structures of pressure and zonal wind of the (1,1,1)-mode	27
7	Total pressure, meridional wind and zonal wind versus colatitude θ of the diurnal (1,1,1)-mode calculated for four different heights. Solid lines: magnitudes; dashed lines: phases	28
8	Horizontal wind field of the (1,1,1)-mode as function of local time on the northern hemisphere	29
8a	Wind field at 100 km corresponding to the wind field of the Hough-function (1, -1) (Kato, 1966)	29
8b	Wind field at 300 km due to solar EUV heat input	29
8c	Wind field at 300 km due to the sum of the EUV heat input and the contribution from the electric field of the S_q current	29
9	Magnitude (Fig. 9a) and phase (Fig. 9b) of the density coefficient $\rho^2_{2,2}/\rho_0$ of the semidiurnal (2,2,2)-mode versus altitude generated by the solar EUV heat input ("EUV), by drag induced coupling ("DR") and by a heat source within the lower atmosphere ("TW"). The dashed lines give the sum of the three contributions	33

ILLUSTRATIONS–(continued)

Figure		Page
10	Magnitude (Fig. 10a) and phase (Fig. 10b) of the temperature coefficient $T^2_{2,2}/T_0$ of the semidiurnal (2,2,2)-mode versus altitude generated by the solar EUV heat input ("EUV"), by drag induced coupling ("DR") and by a heat source within the lower atmosphere ("TW"). The dashed lines give the sum of the three contributions	34
11	Magnitudes (Fig. 11a) and phases (Fig. 11b) of the coefficients of pressure $p^2_{2,2}/p_0$, meridional wind $u^2_{2,2}/c_0$, zonal wind $v^2_{2,2}/c_0$ and vertical wind $w^2_{2,2}/c_0$ of the semidiurnal (2,2,2)-mode versus altitude generated by the sum of the three wave generators considered	36
12	Total pressure, meridional wind and zonal wind versus co-latitude θ of the semidiurnal (2,2,2)-mode calculated for four different heights. Solid lines: magnitudes; dashed lines: phases	37

A NUMERICAL STUDY OF A THREEDIMENSIONAL SPHERICAL THERMOSPHERIC DENSITY AND WIND MODEL

by

H. Volland
Astronomical Institutes
University of Bonn
Bonn, Germany

and

H. G. Mayr
Goddard Space Flight Center
Greenbelt, Maryland

ABSTRACT

Numerical calculations of the generation and propagation of the two important fundamental symmetric tidal wave modes – the diurnal mode (1, 1, 1) and the semidiurnal mode (2, 2, 2) – have been performed applying a realistic model thermosphere and taking into account heat conduction and the temporally and spatially varying ion-neutral collision number. Both wave modes are predominantly generated by the solar EUV heat input. It is shown that the latitude structure of the (1, 1, 1)-mode which is identical with the Hough function (1, -1) within the lower non-dissipative atmosphere degenerates into the spherical function $P_{1,1}$ at thermospheric heights. The pressure field of this mode constitutes the observed pressure bulge of the thermosphere the diurnal component of which peaks at 15 h L. T. in the model of Jacchia and Slowey (1967). Its horizontal wind field agrees with the wind system derived by Kohl and King (1967) and by Geisler (1967). The electric polarization field of the geomagnetic Sq current generates a significant fraction of this wave mode at F layer heights. This wave component shifts the total horizontal wind system to earlier times by about 1 hour in agreement with ionospheric observations. The latitude structure of the (2, 2, 2)-mode is identical with the Hough function (2, 2) within the lower non-dissipative atmosphere. It degenerates to the spherical function $P_{2,2}$ at thermospheric heights. A component of this wave mode generated below 100 km can penetrate deep into the thermosphere and remains significant even at 400 km. Moreover an additional wave component is generated due to non-linear interaction between wave mode (1, 1, 1) and wave mode (2, 2, 2) via ion-neutral collisions at F layer heights. The interference between these two contributions and the XUV generated wave at thermospheric heights causes a phase delay between density and temperature of about 2 hours in the semidiurnal component which contributes to the observed delay between the times of the density and temperature maxima of the neutral gas at thermospheric altitudes.

A NUMERICAL STUDY OF A THREEDIMENSIONAL SPHERICAL THERMOSPHERIC DENSITY AND WIND MODEL

INTRODUCTION

The generation and propagation of tidal and planetary waves within the threedimensional thermosphere has been studied in a previous paper on an approximate base (Volland and Mayr, 1971; referred to as paper I). The main assumptions made there were:

a) Validity of perturbation theory
b) Isothermal atmosphere
c) Consideration of gravity waves only
d) Constant dissipation factors.

In this paper we want to extend this study by abandoning the points (b) to (d). We shall assume a thermosphere model with a realistic temperature profile. We shall introduce heat conduction waves besides the gravity waves and we shall take into account the temporal and spatial distribution of ion-neutral collisions in this model. We shall however again neglect the influence of viscosity waves and shall simulate their effect by an effective height dependent collision number. This study therefore will also be an extension to another previous paper which dealt with a two-dimensional thermospheric model in much the same way (Volland and Mayr, 1970 referred to as paper II).

We shall do numerical calculations of the generation and propagation of two of the most import symmetric tidal waves at thermospheric heights — the fundamental diurnal (1, 1, 1)-mode and the fundamental semidiurnal (2, 2, 2)-mode. We shall study the influence of the solar EUV-heat input into the thermosphere above 100 km on the generation of the two tidal modes. Moreover, we shall estimate the signifiance of waves that are generated within the lower atmosphere below 100 km.

Finally, we shall take into account waves generated by the electric polarization field of the geomagnetic Sq current, by solar semi-diurnal gravitational forces and by non-linear interaction between the (1, 1, 1)-mode and the (2, 2, 2)-mode resulting from the diurnal variation of the ion drag force.

PRECEDING PAGE BLANK NOT FILMED

The abbreviations used in (1) are the following:

T_0, p_0, ρ_0, M_0	mean values of temperature, pressure, density, and molecular mass
T, p, ρ, M	perturbation amplitudes of temperature, pressure density and molecular mass
$\vec{v} = (u, v, w)$	wind vector of the perturbation with its components north-wind u, westwind v, and vertical wind w
$\vec{v}_{hor} = (u, v)$	horizontal component of $\vec{v}$
H_0	pressure scale height within the homogeneous isothermal slab
ν	collision frequency of ion-neutral collisions
u_i, v_i, w_i	components of the ion velocity
θ, λ, r	spherical coordinates
$s = \sin\theta$ $c = \cos\theta$ $z = r - r_0$	height above ground (r_0 = earth's radius)
Ω	angular frequency of the earth's rotation
η	coefficient of molecular viscosity
K	coefficient of molecular heat conductivity
g	gravitational acceleration
c_v	specific heat at constant volumn
Q	heat input component which generates the perturbation
Φ	gravitational tidal potential generating the perturbation.

The collision number ν is a function of time and space. Strictly speaking, it depends on the coupled dynamic system of neutrals and the ionospheric plasma. For convenience we assume ν as an external known function of the form

$$\nu = \nu_{0,0}\, P_{0,0} + \nu_{2,0}\, P_{2,0} + \nu_{1,1}\, P_{1,1} \cos(\tau - \tau_{1,1}) \qquad (2)$$

where $P_{n,m}(\theta)$ are the spherical functions in Neumann's normalization, τ is the local time, $\nu_{n,m}$ (z) are height depending coefficients and $\tau_{1,1}$ is the time of maximum to be specified below.

The ion velocity will be determined from the Lorentz equation in which Coriolis force, inertia and pressure forces and the electron component are neglected:

$$\nu_{in}(\vec{v}_i - \vec{v}) = \frac{e_i}{m_i}(\vec{E} + \vec{v}_i \times \vec{B}) \qquad (3)$$

This leads to the components (with $w \sim 0$)

$$u_i = \frac{1}{\Delta}\{(1 + \delta^2 s^2)\, u - 2\,\delta\, c\, v + (1 + \delta^2 s^2)\,\delta\, u_E - 2\,\delta^2 c\, v_E + 2\,\delta^3 s\, c\, w_E\}$$

$$v_i = \frac{1}{\Delta}\{2\,\delta\, c\, u + v + 2\,\delta^2 c\, u_E + \delta\, v_E - \delta^2 s\, w_E\} \qquad (4)$$

$$w_i = \frac{1}{\Delta}\{2\,\delta^2 s\, c\, u + \delta\, s\, v + 2\,\delta^3 s\, u\, c_E + \delta^2 s\, v_E + (1 + 4\,\delta^2 c^2)\,\delta\, w_E\}$$

with

$$\Delta = 1 + \delta^2 + 3\,\delta^2 c^2$$

$$s = \sin\theta$$

$$c = \cos\theta$$

$$\delta = \frac{\Omega_i}{\nu_{in}} \sim 1.83 \times 10^{-12}\, \frac{\sqrt{M_0}}{\rho_0} \left(\frac{r_0}{r}\right)^3 \begin{cases} \rho_0 & \text{in g/cm}^3 \\ M_0 & \text{in g/mol} \end{cases}$$

$$u_E = \frac{E_\theta}{B_0}; \quad v_E = \frac{E_\lambda}{B_0}; \quad w_E = \frac{E_r}{B_0}$$

$\Omega_i = \frac{e_i B_0}{m_i}$ ion gyro frequency { m_i ion mass; e_i ion charge

$\nu_{in} \sim 1.56\, \rho_0 / M_0^{3/2}$ (Obayashi, 1964)
ion-neutral collision number

$\vec{E} = (E_\theta, E_\lambda, E_r)$ electric field vector

$B_0 \sim 3 \times 10^{-5}$ V s/m^2 magnetic induction of the earth's co-axial dipole field at the equator.

At heights above the dynamo region, the electric field is orthogonal to the geomagnetic lines of force ($w_E = - s\, u_E/2c$), and it is $\delta >> 1$.

Thus,

$$u_i \sim \frac{s^2 u - 2 c v_E}{1 + 3 c^2}$$

$$v_i \sim \frac{u_E}{2 c} \qquad \text{at } z \gtrsim 150 \text{ km}$$

$$w_i \sim \frac{2 s c u + s v_E}{1 + 3 c^2}$$

Here, the wind induced component of the ion movement is primarily bound to the geomagnetic lines of force along which momentum can be transferred from the neutral to the ionized component.

Within the dynamo region it is $\delta << 1$, and (4) becomes

$$u_i \sim u$$
$$v_i \sim v \quad \text{at} \quad z < 130 \text{ km}, \tag{6}$$
$$w_i \sim 0$$

and the ions essentially move with the neutral wind.

A more sophisticated study has to take into account the electron component within the dynamo region (see e.g., Kato and Matsushita, 1969). However, since the ion-neutral drag becomes significant for the neutral gas dynamics mainly above the dynamo region we shall neglect those complications and shall use Eq. (4) in the whole altitude range above 100 km.

3. DEVELOPMENT IN TERMS OF TIDAL MODES

It is well known from tidal theory that only a discrete number of eigenfunctions or tidal wave modes (the so-called Hough-functions) can exist within the atmosphere (e.g., Chapman and Lindzen, 1970). These eigenfunctions will be written as (see Paper I)

$$E^f_{n,m} = \Theta^f_{n,m} \exp (j\, m \lambda + j\, f\, \Omega\, t) \tag{7}$$

with

$$\Theta^{f\ *)}_{n,m} = \sum_{n'} \delta^f_{n,n',m}\, P_{n',m}\,(c) \tag{7a}$$

Here it is

$$f = \frac{1}{\Omega}(\omega + s\, \Omega_a) \quad \text{a normalized frequency}$$

---

* In this paper we introduced for convenience spherical functions in Neumann's normalization. However, in paper I we used the spherical functions in Schmidt's normalization. It is

$$\left.\begin{matrix}\Theta^{m,f}_n \\ P^m_n\end{matrix}\right\} = \sqrt{\frac{2\,(n-m)!}{(n+m)!}} \left\{\begin{matrix}\Theta^f_{n,m} \\ P_{n,m}\end{matrix}\right. \quad \text{and} \quad \delta^{m,f}_{n,n'} = \sqrt{\frac{(n'+m)!}{(n'-m)!}\,\frac{(n-m)!}{(n+m)!}}\,\delta^f_{n,n',m}$$

ω the angular frequency of the wave

Ω the angular frequency of the earth's rotation

Ω_a the angular frequency of the earth's orbital rotation

t universal time

n, m, s integers specifying the type of the wave mode

$\delta^f_{n,n',m}$ coefficients of Θ_n to be determined below

$\delta^f_{n,n,m} = 1.$

The Hough-function of type (n, m, f) is determined from the eigenvalue problem of the two homogeneous equations (1b) and (1c) (setting $\vec{E} = \Phi = 0$) together with

$$\mathrm{div}\,\{v_{hor}\}^f_{n,m} + \frac{j\,f\,\Omega H_0}{h^f_{n,m}}\,\frac{p^f_{n,m}}{p_0}\,E^f_{n,m} = 0 \qquad (8)$$

Here, $h^f_{n,m}$ is the so-called equivalent depth and $p^f_{n,m}$ is the pressure amplitude of the wave mode of type (n, m, f).

The electric field $\vec{E}$ and the gravitational potential Φ are considered as external forces, although strictly speaking, $\vec{E}$ in the case of the electric potential of the Sq current is generated itself by the neutral wind at E-layer heights. However, the energy necessary to generate $\vec{E}$ is only a small fraction of the kinetic energy of the driving wind which partly even originates below 100 km altitude. Therefore, at E-layer heights this small fraction of the kinetic energy does not significantly influence the wind itself, and $\vec{E}$ can be calculated independently from the dynamo theory. However, $\vec{E}$ affects the neutral wind at F layer heights where the electromagnetic energy is here of the same order of magnitude as the kinetic energy of the wind. $\vec{E}$, therefore, acts like a coupling link between E- and F-layer regions coupling a fraction of the kinetic energy of the wind at E-layer heights into the F-layer region. $\vec{E}$ tries to map the wind structure at E-layer heights into the upper part of the thermosphere.

We shall determine the eigenvalue problem in the next sections. Here we shall assume that the equivalent depth $h^f_{n,m}$ and the coefficients $\delta^f_{n,n',m}$ of $\Theta^f_{n,m}$ are already known. Then, the perturbation amplitudes ρ, p, T, w and M as well as the heat input Q can be developed in terms of the wave modes $E^f_{n,m}$:

$$\left.\begin{matrix}\rho\\ p\\ T\\ w\\ M\\ Q\end{matrix}\right\} = \sum_{n,\,m,\,f} \left\{\begin{matrix}\rho^f_{n,m}\\ p^f_{n,m}\\ T^f_{n,m}\\ w^f_{n,m}\\ M^f_{n,m}\\ Q_{n,m}\end{matrix}\right\} E^f_{n,m} \tag{9}$$

Likewise the electric field components and the gravitational potential may be developed in terms of the eigenfunctions. We find then from (1b) and (1c)

$$\mathrm{div}\,\vec{v}_{hor} = -\,j\,\Omega \sum_{n,m,f} \left\{ \frac{f\,H_0\,p^f_{n,m}}{p_0\,h^f_{n,m}} + F\,e^f_{n,m} + F\,g^f_{n,m} \right\} E^f_{n,m} \tag{10}$$

Here, $F\,e^f_{n,m}$ and $F\,g^f_{n,m}$ are functions of the components of the electric field and of the gravitational potential, respectively. They will be determined in the following sections.

4. THE VERTICAL STRUCTURE FUNCTION

Introducing (9) and (10) into (1a), (1d), (1e) and (1f) allows to separate the various wave modes, and we obtain after elimination of ρ from (1f) a system of four inhomogeneous linear ordinary differential equations of first order. They describe the altitude dependence of vertical wind $w^f_{n,m}$, pressure $p^f_{n,m}$, temperature $T^f_{n,m}$ and vertical heat flux $F^f_{n,m} = K\,d\,T^f_{n,m}/dz$ of the perturbation amplitudes of wave mode (n, m, f) which we write in concise matrix form

$$\frac{1}{j\,k_0}\,\frac{d\,\underline{e}}{d\,z} = \underline{K}\,\underline{e} + \underline{h} \tag{11}$$

with

$$\underline{e} = \sqrt{p_0\, c_0} \begin{pmatrix} w^f_{n,m}/c_0 \\ p^f_{n,m}/p_0 \\ T^f_{n,m}/T_0 \\ F^f_{n,m}/(p_0\, c_0) \end{pmatrix} \tag{11a}$$

$$\underline{K} = \begin{pmatrix} -jA & -f(1 - H_0/h^f_{n,m}) & f & 0 \\ 0 & jA & -2jA & 0 \\ 0 & 0 & jA & -2j\kappa G \\ -2jA & -f & f/\kappa & -jA \end{pmatrix} \tag{11b}$$

$$\underline{h} = \sqrt{p_0\, c_0} \begin{pmatrix} F\, e^f_{n,m} + F\, g^f_{n,m} - f\, F\, m^f_{n,m} \\ 2jA\, F\, m^f_{n,m} \\ 0 \\ j\, J^f_{n,m}/\kappa - f\, F\, m^f_{n,m} \end{pmatrix} \tag{11c}$$

$$J^f_{n,m} = \frac{\kappa\, Q^f_{n,m}}{\Omega\, p_0}; \quad G = \frac{\gamma\, g}{2\, V_0}; \quad V_0 = \frac{K\, g}{c_p\, p_0}; \quad \kappa = \frac{\gamma - 1}{\gamma}$$

$$F\, m^f_{n,m} = \frac{M^f_{n,m}}{M_0}; \quad A = \frac{\gamma\, g}{2\, c_0} = \frac{1}{2\, k_0\, H_0}; \quad k_0 = \frac{\Omega}{c_0}.$$

γ = ratio between the specific heats at constant pressure and constant volume

$c_0 = \sqrt{g\, \gamma\, H_0}$ = velocity of sound.

The solution of (11) is straight forward and is fully described in paper II. Essentially, the procedure is to divide the real atmosphere into a number of homogeneous and isothermal slabs in which the elements of the matrices $\underline{K}$ and $\underline{h}$ are constant. Then one can transfer the physical parameters $\underline{e}$ in (11) into the characteristic waves:

$$\underline{e} = \underline{Q}\,\underline{c} \tag{12}$$

where $\underline{Q}$ is a transformation matrix and

$$\underline{c} \begin{pmatrix} a_1 \\ a_2 \\ b_1 \\ b_2 \end{pmatrix} \tag{13}$$

contains upgoing (a) and downgoing (b) waves of gravity wave type (i = 1) and heat conduction wave type (i = 2) the height dependence of which is

$$\left.\begin{matrix} a_1 \\ b_i \end{matrix}\right\} \propto \exp\left(\pm\, j\, k_0\, q_i\, z\right) \tag{14}$$

with the eigenvalues

$$q_i = \sqrt{-A^2 - j\, f\, G \mp \sqrt{-f^2 G^2 + 8\, j\, f\, \kappa\, G\, A^2\, H_0/h^f_{n,m}}} \tag{15}$$

The upper (negative) sign in the square root of (15) belongs to the gravity waves while the lower (positive) sign belongs to the heat conduction waves. This eigenvalue has the same form as the eigenvalue of plane inertial waves (with $A^2, G \gg \gamma, S^2$) if we replace

$$H_0/h^f_{n,m} = k_x^2/k_0^2\, \gamma\, f^2 = S^2/\gamma \tag{16}$$

where k_x is the horizontal wave number of the plane waves (Pitteway and Hines, 1963). However, contrary to plane waves, the tidal waves have only a discrete number of (generally complex) horizontal wave numbers.

Such transformation from the physical parameters into the characteristic waves as well as the slab method have the advantage that analytic solutions exist appropriate for numerical calculations and that the radiation condition can be adopted as boundary condition (see paper II).

The inhomogeneous term $\underline{h}$ in (11) is responsible for the excitation of the wave mode. It contains the external forces due to heat input $J^f_{n,m}$, electric fields $F\,e^f_{n,m}$ and tidal gravitational potential $F\,g^f_{n,m}$. Since our system (11) is linear, particular solutions of (11) can be superimposed to give the complete solution. Thus, we are able to separate the influence of the various excitation mechanisms by setting all but one of the elements J, Fe and Fg equal to zero.

There remains the additional term $F\,m^f_{n,m}$ in (11c) which describes the temporal and spatial variation of the mean molecular mass. It is only a fictive external source because this variation is generated by the dynamic processes within the thermosphere and therefore is originally generated by the real external forces. As it is well known, the thermosphere is neither completely mixed nor in a complete diffusion equilibrium. An exact calculation of the thermosphere dynamics including diffusion processes must therefore be based upon the coupled system of hydrodynamic and diffusion equations for the various constituents.

In the following calculations we shall neglect the term $F\,m^f_{n,m}$ because it can be shown that F m does not influence significantly the pressure and density amplitude of the tidal waves.

It follows then from (1f) that the magnitude of the temperature becomes increased by Fm. Therefore, in the following results our relative temperature amplitudes may be underestimated as the result of the neglect of the variation of the molecular mass.

5. THE DETERMINATION OF THE EIGENFUNCTIONS

We now return to the remaining problem of determining the eigenfunctions and the equivalent depths of the tidal modes. In paper I, we used an approximate way to calculate the coefficients $\delta^f_{n,n',m}$ of the eigenfunctions $\theta^f_{n,m}$ and the equivalent depths $h^f_{n,m}$. The assumptions made were the following:

a) Replacement of the viscosity force by an effective Rayleigh friction parameter:

$$-\frac{\partial}{\partial z}\left(\eta \frac{\partial}{\partial z}\begin{Bmatrix} u \\ v \end{Bmatrix}\right) \sim Z_{vis}\, \Omega\, \rho_0 \begin{Bmatrix} u \\ v \end{Bmatrix} \tag{17}$$

where Z_{vis} is a positive height denpendent number.

b) Collision number ν only height dependent

c) Zero ion velocity.

Here, point (a) is the most restrictive one because it is equivalent to an outfiltering of two kinds of characteristic waves, the so-called viscosity waves, which mainly influence the horizontal velocity. We shall retain point (a) because otherwise the mathematical difficulties would become overwelming. Moreover, it can be shown that the number Z_{vis} is small when compared with the corresponding ion drag term

$$Z_{col} = \nu/\Omega \tag{18}$$

below 300 km. Therefore, viscosity has in fact not much influence on thermosphere dynamics in that height range (Geisler, 1967; Kohl and King, 1967). At greater heights, however, the viscosity tends to keep the horizontal velocity constant with altitude. It is possible to simulate this influence by an effective collision number above 300 km altitude (see paper II).

We want now to abandon points (b) and (c) in our treatment. We shall show explicitly the way to do this for the fundamental symmetric tidal mode (1, 1, 1) which is the trapped mode (1, -1) within the lower atmosphere according to Kato (1966). The treatment of the other tidal modes follows the same line.

In the case that points (a) to (c) were applied we found in paper I the solutions for pressure amplitude p and horizontal winds u and v of wave mode (1, 1, 1) (n = 1; m = 1; f = 1) from Eqs. (1b), (1c) and (17)

$$p = (p^1_{1,1} P_{1,1} + p^1_{3,1} P_{3,1})\, e^{j\tau}$$

$$u = u^1_{1,1} \frac{P_{2,1}}{\sin\theta}\, e^{j\tau} \tag{19}$$

$$v = (v^1_{1,1} P_{1,1} + v^1_{3,1} P_{3,1}) \frac{e^{j\tau}}{\sin\theta}$$

with

$$u^1_{1,1} = \frac{(f_k + 2/3)\ j}{3\gamma\xi\Delta} \frac{c_0}{p_0} p^1_{1,1}; \quad v^1_{1,1} = \frac{(f_k - 14/15)}{\gamma\xi\Delta} \frac{c_0}{p_0} p^1_{1,1}$$

$$p^1_{3,1} = -\frac{8}{45\Delta} p^1_{1,1}; \quad v^1_{3,1} = \frac{4}{15(f_k - 14/15)} v^1_{1,1};$$

$$\Delta = f_k^2 - 4 f_k/3 - 4/15$$

$$\xi = \frac{\Omega}{c_0} r; \quad f_k = 1 - j(Z_{vis} + Z_{col}); \quad \tau = \Omega t + \lambda \ \text{(local time)}.$$

From Eq. (10) it follows according to paper I (Eq. II/7) approximately

$$h^1_{1,1} = \frac{\Omega^2 r^2 \Delta}{2g(f_k - 1/3)}, \tag{20}$$

We retain in the following the general form of (19), however with coefficients to be determined below. Moreover, we introduce

$$\begin{matrix} \nu(u - u_i) \\ \nu(v - v_i) \end{matrix} = \frac{\Omega}{\sin^q\theta} \sum_{f=0}^{2} \sum_{r} (A^f_{r,1} u^1_{1,1} + B^f_{r,1} v^1_{1,1} + d^f_{r,1}) P_{r,f} e^{jf\tau} \tag{21}$$

with

$$q = \begin{cases} 1 & r \geq 1 \\ \text{for} & \\ -1 & r = 0. \end{cases}$$

Here, for the meridional component u, it is r = 2, 4, 6 . . . , and for the zonal component v, it is r = 1, 3, 5 . . .

The coefficients $A^f_{r,1}$ and $B^f_{r,1}$ can be derived from (2) and (4) applying well known theorems of spherical functions. For example it is

$$A^1_{r,1} = \frac{(2\,r+1)}{r\,(r+1)\,\Omega} \int_0^1 \frac{\nu_{0,0} - \nu_{2,0}/2 + 3\,\nu_{2,0}\,c^2/2)}{(1+\delta^2+3\,\delta^2\,c^2)}\, P_{2,1}\, P_{r,1}\, dc \begin{cases} 4\,\delta^2\,c^2 \\ -2\,\delta\,c \end{cases}$$

$$\text{for} \begin{cases} r = 2\,n' \\ r = 2\,n'+1 \end{cases} \tag{22}$$

Similar formulas exist for the coefficients $B^1_{r,1}$. The integration of (22) is straightforward.

The electric polarization fields in (4) give rise to the coefficients

$$d^1_{r,1} = \frac{(2\,r+1)}{r\,(r+1)\,\Omega} \int_0^1 e^{-j\tau\,(\nu_{0,0} - \nu_{2,0}/2 + 3\,\nu_{2,0}\,c^2/2)}\, s\, P_{r,1}\, dc \begin{cases} \dfrac{2\,c\,v_E}{1+3\,c^2} \\ -\dfrac{u_E}{2\,c} \end{cases}$$

$$\text{for } n = \begin{cases} 2\,n' \\ 2\,n'+1 \end{cases} \quad \text{and} \quad z \gtrsim 150 \text{ km} \tag{23}$$

$$d^1_{r,1} \sim 0 \quad \text{for} \quad z < 150 \text{ km}.$$

The last assumption is reasonable because, below 150 km, it is $d^1_{r,1} \propto \delta\,\nu_{0,0}$. δ and $\nu_{0,0}$ are both small in this height range.

In (23), the electric polarization field is due to the Sq current and has the form (Volland, 1971)

$$u_E = -3\,c\,(1 - 2\,c^2)\; j\; V^e\; e^{j\tau}$$

$$v_E = -(1 + 2\,c^2)\; V^e\; e^{j\tau} \qquad (24)$$

with

V^e = 40 m/sec during moderate solar activity

$c = \cos\theta$; $s = \sin\theta$; c_0 = velocity of sound

τ local time, zero at midnight.

Since the symmetric diurnal component of the solar gravitational tidal potential is zero (Chapman and Lindzen, 1970), we set furthermore

$$\Phi^1_{1,1} = 0. \qquad (25)$$

For the moment we shall neglect the series with the periods 0 and 2τ on the right hand side in (21). We shall discuss their influence later. Introducing now (17), (19), (21), and (25) into (1b) and (1c), applying well known formulas of spherical harmonics and truncating the development into series of spherical harmonics after the terms with n = 4, we obtain from (1b) and (1c) four linear inhomogeneous equations for the coefficients $u^1_{1,1}$, $v^1_{1,1}$, $v^1_{3,1}$ and $p^1_{3,1}$ with the solutions

$$\left.\begin{matrix} u^1_{1,1} \\ v^1_{1,1} \\ v^1_{3,1} \\ p^1_{3,1} \end{matrix}\right\} = a_i\; p^1_{1,1} + b_i\; V^e \quad (i = 1,\ 2,\ 3,\ 4) \qquad (26)$$

Eliminating the wind components of (26) in (10) and applying the same approximation as in paper I (Eq. II/7), we obtain the equivalent depth and the external forces

$$h^1_{1,1} = -\frac{2\,\xi\,H_0\,c_0}{3\,p_0\,(j\,a_1 + a_2 + a_3)}$$

$$F\, g^1_{1,1} = 0$$

$$F\, e^1_{1,1} = \begin{cases} -\dfrac{3}{2\xi}(j\, b_1 + b_2 + b_3)\dfrac{V^e}{c_0} & \text{for } z \gtrsim 150 \text{ km} \\ \sim 0 & < 150 \text{ km} \end{cases} \qquad (27)$$

Evidently, the accuracy of this method depends on the degree of truncation of the series of spherical harmonics and can in principle be improved by taking into account higher order terms in the series.

6. MODE COUPLING

In our treatment, we use perturbation theory and neglect products of the wave parameters as small values. Thus, we eliminate any coupling between modes of different wave domain numbers (n, m, f). An estimate about the contributions of the non-linear terms led to magnitudes not greater than 20% of the linear terms (see paper I). Such errors should be tolerable in view of the complex problem. In spite of perturbation theory, we expect two other coupling mechanisms between the various modes. The first one is due to the diurnal variation of the collision number ν in (4). The second one is related to the change with height of the latitude structure of the eigenfunctions.

We first consider the effect of collisions. In (21) we already added two series with periods zero and 2τ which followed from products of the kind

$$P_{1,1}\, \nu_{1,1} \cos(\tau - \tau_{1,1})\, P_{1,1}\, |u^1_{1,1}| \cos(\tau - \tau^1_{1,1}) \qquad (28)$$

and equivalent expressions for the zonal wind component $v^1_{1,1}$. The determination of the coefficients in (21) was outlined in section 5. Evidently, the coefficients $A^0_{r,1}$, $A^2_{r,1}$ etc. lead to mode coupling from the (1, 1, 1)-mode into the semi-diurnal (n, 2, 2)-modes and the planetary (n, 0, 0)-modes with periods 2τ and zero, respectively. This coupling does not affect the (1, 1, 1)-mode itself.

On the other hand, the modes (n, 2, 2) and (n, 0, 0) couple part of their energy into the (1, 1, 1)-mode via neutral collisions. From the observations of thermospheric density variations, it is obvious (Jacchia and Slowey, 1967) that in the case of the symmetric modes only the modes (2, 0, 0) and (2, 2, 2) have significant amplitudes besides the dominant (1, 1, 1)-mode. The degree of coupling can be estimated from the ratios

$$\frac{\nu_{1,1}\,(u)^{0}_{2,0}}{2\,\nu_{0,0}\,(u)^{1}_{1,1}} \quad \text{and} \quad \frac{\nu_{1,1}\,(u)^{2}_{2,2}}{2\,\nu_{0,0}\,(u)^{1}_{1,1}} \tag{29}$$

where $(u)^{f}_{n,m}$ are the maximum amplitudes of the meridional winds of the respective modes, and the factors 2 stand for the splitting of products of the kind (28) into modes of period τ and 3τ.

Assuming $\nu_{0,0} \sim \nu_{1,1}$, we estimate from the result of paper I ratios of (29) of 0.05 and 0.15, respectively. They are smaller than the contributions from the non-linear terms of the wave parameters. Thus, it is justified to neglect this coupling into the (1, 1, 1)-mode due to ion-neutral colllsions. On the other hand, the coupling from the (1, 1, 1)-mode into the modes (2, 0, 0) and (2, 2, 2) expressed in the two series in (21) is by no means negligibly small. It acts like an "external" force for the generation of these two modes.

The second kind of mode coupling occurs in connection with the height change of the latitude structure of the eigenfunctions as we see this for example from the coefficient

$$a_4 = -\frac{8}{45\,(f_k^2 - 4\,f_k/3 - 4/15)} \tag{30}$$

of the (1, 1, 1)-mode (see Eq. (19) and (26)). Even in the simplest case of (19) is f_k a function of altitude. Within the lower atmosphere, it is $f_k = 1$ and $a_4 = 0.3$. Above about 200 km, it is $|f_k| >> 1$, and $|a_4| < 0.05$. It is the altitude range between 100 and 200 km, where the change of the latitude structure of the modes is most drastical (see Fig. 6).

This altitude dependence of the mode structure is however in contradiction to the method of the separation of the variables applied in this paper which presupposes the eigenfunctions $\Theta^{f}_{n,m}$ to be altitude independent. The effect of this altitude dependence is that, at any height, part of the energy of the modes is either partially refelcted or transferred into an other mode of the same wave domain number n. Unfortunately, this mode coupling is a completely open problem and not yet solved. One can perhaps argue that because of the observed insignificant contributions of the modes with wave domain numbers $n > 2$ at thermospheric heights the degree of coupling from the higher order modes into modes of lowest wave domain numbers should be very small, whereas on the other hand the thermosphere filters out the higher order modes which are generated due to this coupling from the lowest order modes. We shall not try to estimate the degree of coupling in this paper but rather leave it to further studies.

7. THE FUNDAMENTAL SYMMETRIC DIURNAL TIDAL MODE (1,1,1)

We are now prepared to do numerical calculations for the generation and the propagation of tidal waves at thermospheric altitudes. We shall restrict ourselves in this paper to the two important symmetric modes: the fundamental diurnal tidal (1,1,1)-mode and the fundamental semi-diurnal mode (2,2,2)-mode. In this section we start with the diurnal mode (1,1,1).

We select as in paper I a height profile of the mean collision number plotted in Figure 1 as solid line which is roughly proportional to the electron

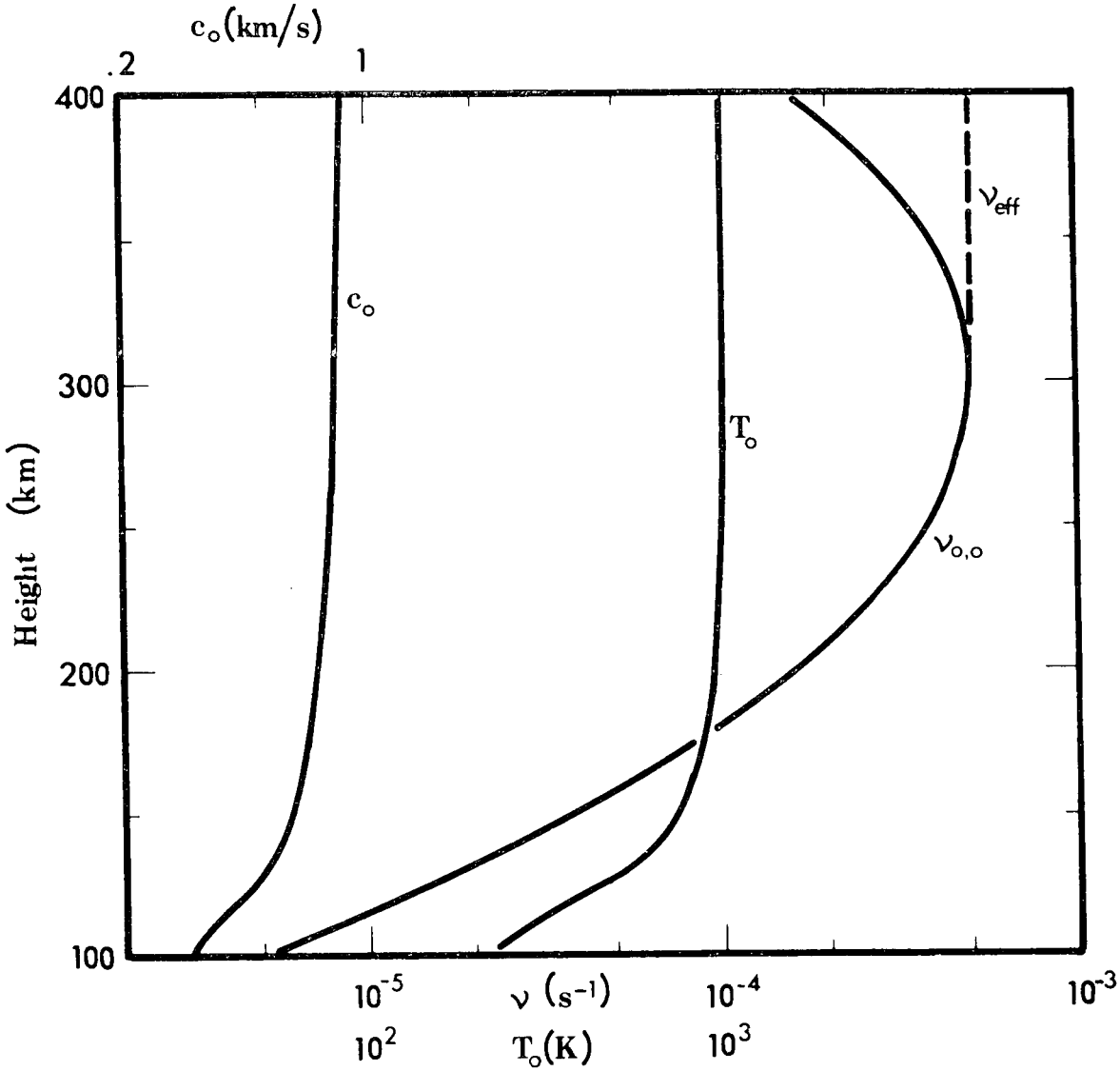

Figure 1. Height profiles of mean temperature T_0, mean velocity of sound c_0, mean collision number $\nu_{0,0}$ and effective collision number ν_{eff} used in the model calculations.

density. Above 300 km we add to this collision number a Rayleigh friction term $\nu_{vis} = \Omega Z_{vis}$ (see Eq. (17)) which simulates the influence of molecular viscosity. The sum $\nu_{eff} = \nu_{0,0} + \nu_{vis}$ is constant above 300 km (the dashed line in Fig. 1).

The spatial and temporal distribution of the collision number is given by Eq. (2) with the coefficients

$$\nu_{2,0} = -0.76\, \nu_{0,0}$$

$$\nu_{1,1} = \nu_{0,0}$$

$$\tau_{1,1} = 12 \text{ h L.T.}$$

The mean temperature T_0, the mean pressure p_0 and the mean molecular mass M_0 are taken from the Jacchia model (Jacchia, 1965) for an exospheric temperature of $T_\infty = 1000°K$. The temperature and the velocity of sound for this model are plotted in Figure 1 versus altitude.

As solar heat input we adopted three height profiles:

$$Q_I \propto p_0$$

$$Q_{II} \propto \exp(-z/H); \quad (H = 50 \text{ km}) \tag{31}$$

$$Q_{III} \propto \begin{cases} p_0 & z \geq 160 \text{ km} \\ \text{for} & \\ \exp(-z/H); \quad (H = 27.5 \text{ km}) & z < 160 \text{ km} \end{cases}$$

Below 100 km the heat input is taken as zero. In all three cases maximum heat input occurs at 12.00^h local time. The heat input Q_I was used in paper I, the heat input Q_{II} was used in paper II.

The height profiles of these three heat inputs are plotted in Figure 2. The numbers $\bar{E}_i$ give the total heat input per volume and time above 100 km:

$$\bar{E}_i = \int_{z_0 = 100\,\mathrm{km}}^{\infty} Q_i \, d z \; (\mathrm{erg/cm^2\ sec}). \tag{32}$$

These numbers are chosen such that the corresponding density amplitudes at 400 km altitude agree with the observed data.

Figure 3 show the coefficient $\rho^1_{1,1}/\rho_0$ of the relative density amplitude in magnitude (Fig. 3a) and phase (Fig. 3b) versus altitude generated by the respective

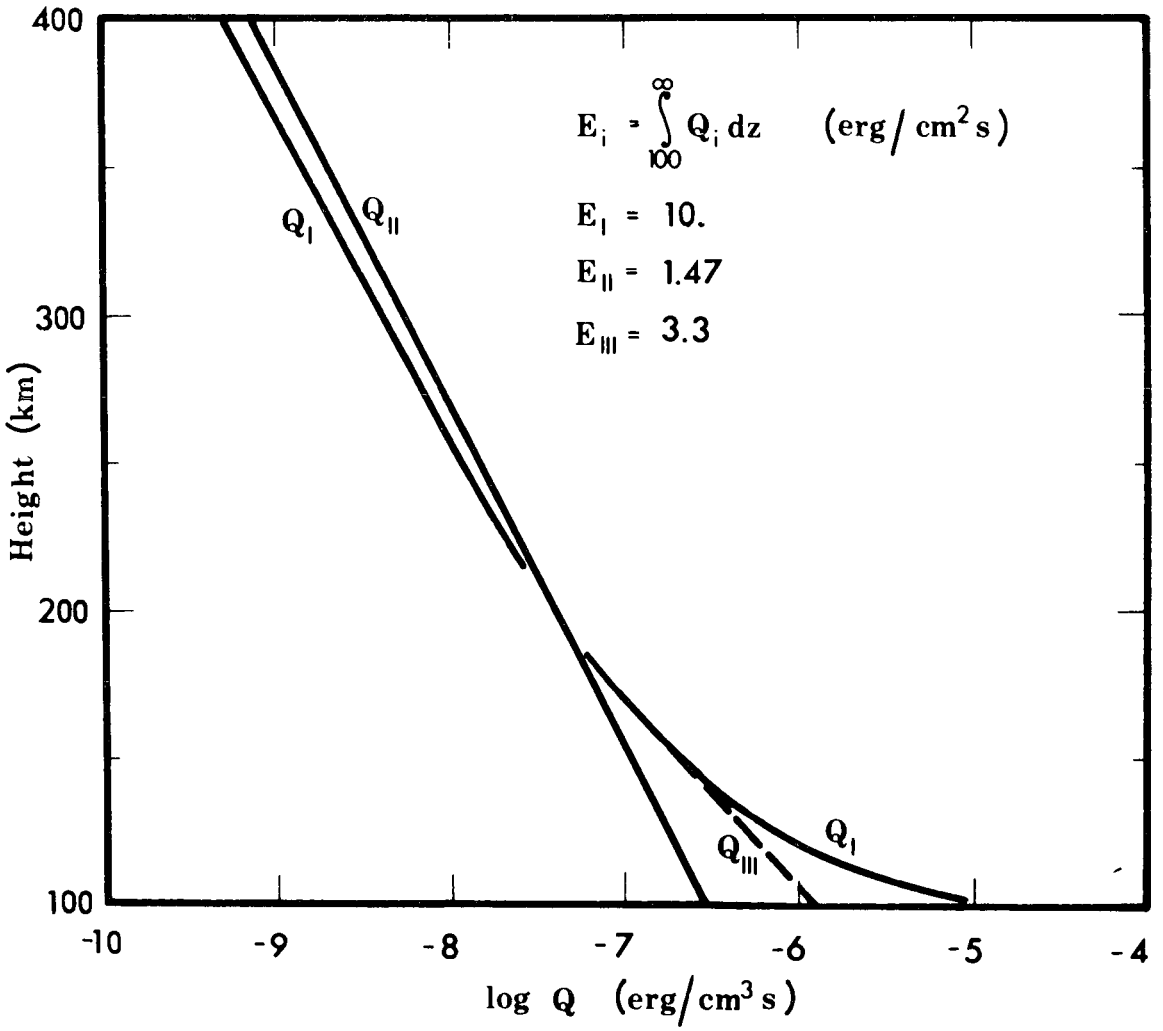

Figure 2. Solar EUV heat input Q_i versus altitude used in the model calculations.

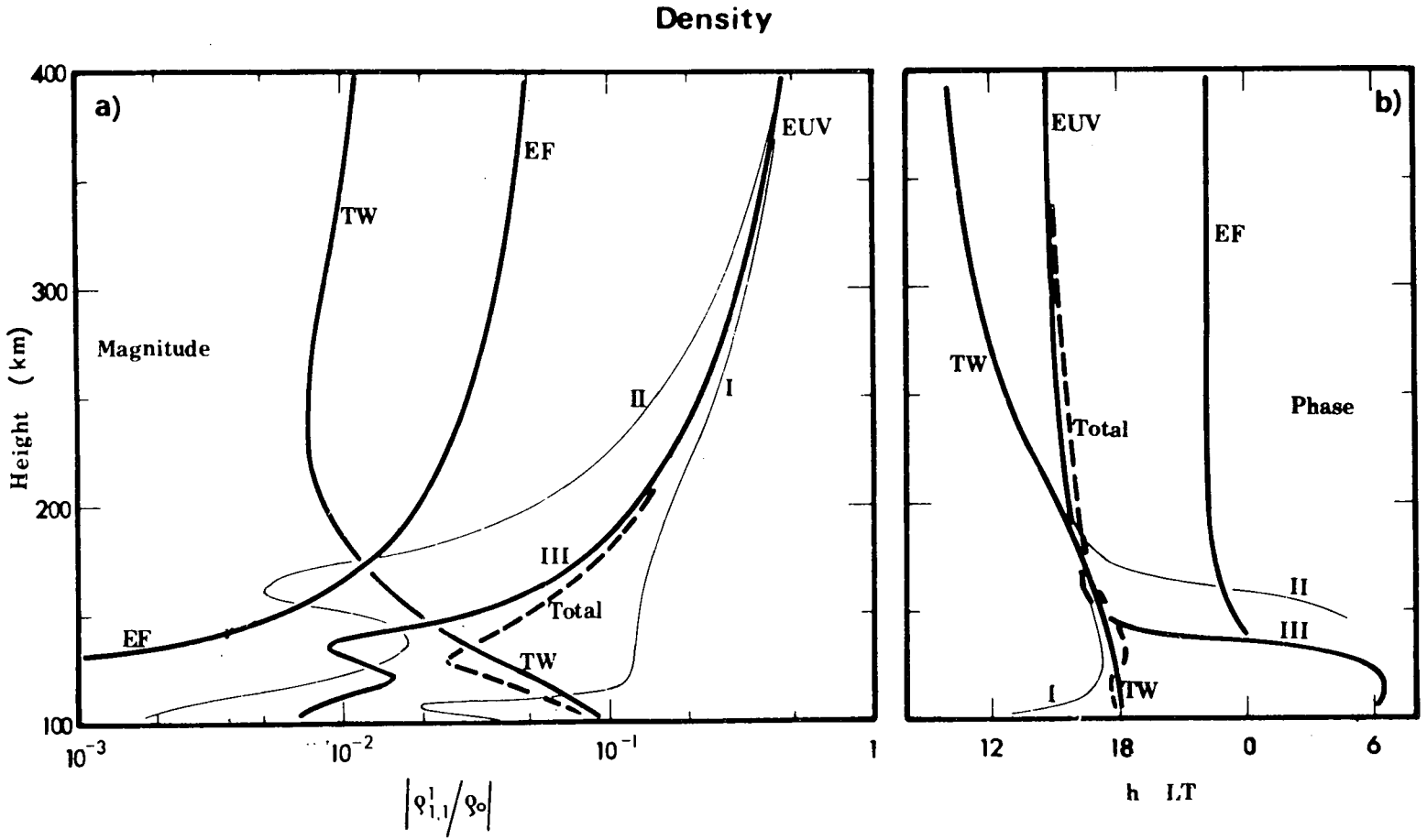

Figure 3. Magnitude (Fig. 3a) and phase (Fig. 3b) of the density coefficient $\rho^1_{1,1}/\rho_0$ of the diurnal (1, 1, 1)-mode versus altitude generated by solar EUV heat input Q_{111} ("EUV"), by the electric field of the Sq current ("EF") and by a heat source within the lower atmosphere ("TW"). The dashed lines give the sum of the three contributions. The thin solid lines have been calculated adopting heat sources Q_1 and Q_{11} from Fig. 2.

three heat sources Q_I, Q_{II} and Q_{III} (Symbols: I, II and III). Also plotted in Figure 3 is the density of a free internal upward propagating wave with magnitude $|\rho^1_{1,1}|/\rho_0 = 0.1$ and time of maximum of 18.00^h L.T. at 100 km altitude (Symbol: T.W). Finally, the density amplitude due to the electric polarization fields of the geomagnetic Sq current generated by the term $Fe^1_{1,1}$ in (27) is plotted in Fig. 3. (Symbol: "EF"). From Fig. 3a we notice that the wave from below decays rapidly between 100 and 200 km and becomes insignificant above about 180 km altitude. This is contrary to the result in paper II where we overestimated the influence of the wave from below due to the neglect of the Coriolis force. However, above 230 km the wave from below although of insignificant amplitude again increases slowly with height which is in agreement with the result of the two dimensional model in paper II. It shows the negligible influence of the Coriolis force on wave propagation in that height range. The density amplitude excited by the electric Sq field is only a small fraction of the total density amplitude in the entire altitude range considered and generally can be neglected. In the case of the wave generated by the solar XUV-heat input, we know from the geomagnetic Sq variations that the corresponding maximum horizontal wind between 100 and 200 km is of the order of 100 m/sec and the relative density amplitude of the order of 0.05. (Kato, 1956, 1966). The same order of magnitude of the density variations is determined from rocket born and satellite drag observations (Spencer et al., 1966; Taeusch et al., 1968; King-Hele and Hingston, 1967, 1968). These facts suggests that heat source III may give the best fit to the observations. The total density amplitude is the sum of the component generated by the XUV-heat input Q_{III}, the electric field induced component and the wave from below. It is plotted as thick dashed line in Fig. 3. Evidently, the wave from below predominates within the first 50 km above our lower boundary of the model.

The total heat energy of heat source III above 100 km is $\bar{E}_{III} = 3.3$ erg/cm sec. This value is at the upper limit of the results of Hinteregger et al. (1965) from observations of the solar spectrum which is another reason to exclude heat source I. According to Hays (1970) the effective solar heat input is roughly proportional to the mean pressure. Our calculations show that this appears to be a reasonable approximation above E-layer heights. Within the E-region however it seems to be too high. Our normalized heat input $J^1_{1,1}$ introduced in (11c) is

$$J^1_{1,1} = 0.17 \text{ at } z \geq 160 \text{ km} \tag{33}$$

This value is greater by a factor of at least 40 when compared with the corresponding number within the Ozone layer at stratospheric heights (Chapman and

Lindzen, 1970). At 100 km, this value reduces by a factor of 10 to $J^1_{1,1} = 0.017$ which is still greater by a factor of 4 when compared with the Ozone layer source.

The amplitude of the wave from below in Fig. 3a corresponds to a heat input of $J^1_{1,1} = 0.017$ within the entire lower nondissipative atmosphere below 100 km. Because the estimated energy input seems much smaller at stratospheric heights, this may be an overestimate. However, since the penetration depth of this evanescent wave is limited to a few scale heights, only the heat input into the mesosphere and into the lower thermosphere accounts actually for the amplitude of this wave at 100 km altitude, and the exact number of this heat input is not known.

In Fig. 3b we plotted the time of maximum of the density versus altitude. The XUV-generated wave peaks between 14 and 15 hours local time above 250 km altitude which is in agreement with the satellite drag data (e.g. Jacchia and Slowey, 1967). Below 150 km where the wave from below predominates the time of maximum shift toward 18 hours local time. A density maximum between 16 and 18 hour is just necessary to explain the phase of the Sq current (Tarpley, 1970; Volland, 1971). The electric field induced density component peaks near 22 hours local time above 180 km and shifts the total density maximum to 15 hours at 400 km altitude.

In Fig. 4a we plotted versus altitude the magnitudes of the normalized meridional wind components $u^1_{1,1}/c_0$ which are generated by the EUV heat input (heat source III in (31)), by the electric field of the Sq current and by the wave from below. The dashed line gives the sum of all three contributions. Here the electric field induced wave has the same order of magnitude as the EUV-induced wave at F2 layer heights. The wave from below dominates below 130 km and becomes insignificant above 160 km. The reason for the difference between the large wind amplitude and the small amplitude of density (and therefore pressure, temperature and vertical wind) of the electric field induced wave (see Fig. 3a) is that the electric field induced component of the horizontal wind field is nearly divergence free which implies a very small driving term Fe for the pressure in (27).

The phases of the meridional winds shown in Fig. 4b vary between about 21^h and 5^h local time above 120 km. The phase of the total wind remains between 0^h and 2^h local time in the height range from 100 to 400 km. This is just the phase necessary to explain the phase of the geomagnetic Sq current (Tarpley, 1970).

In Fig. 5 we plotted magnitudes and phases of the relative amplitudes of pressure $p^1_{1,1}/p_0$, temperature $T^1_{1,1}/T_0$, vertical wind $w^1_{1,1}/c_0$ and zonal wind

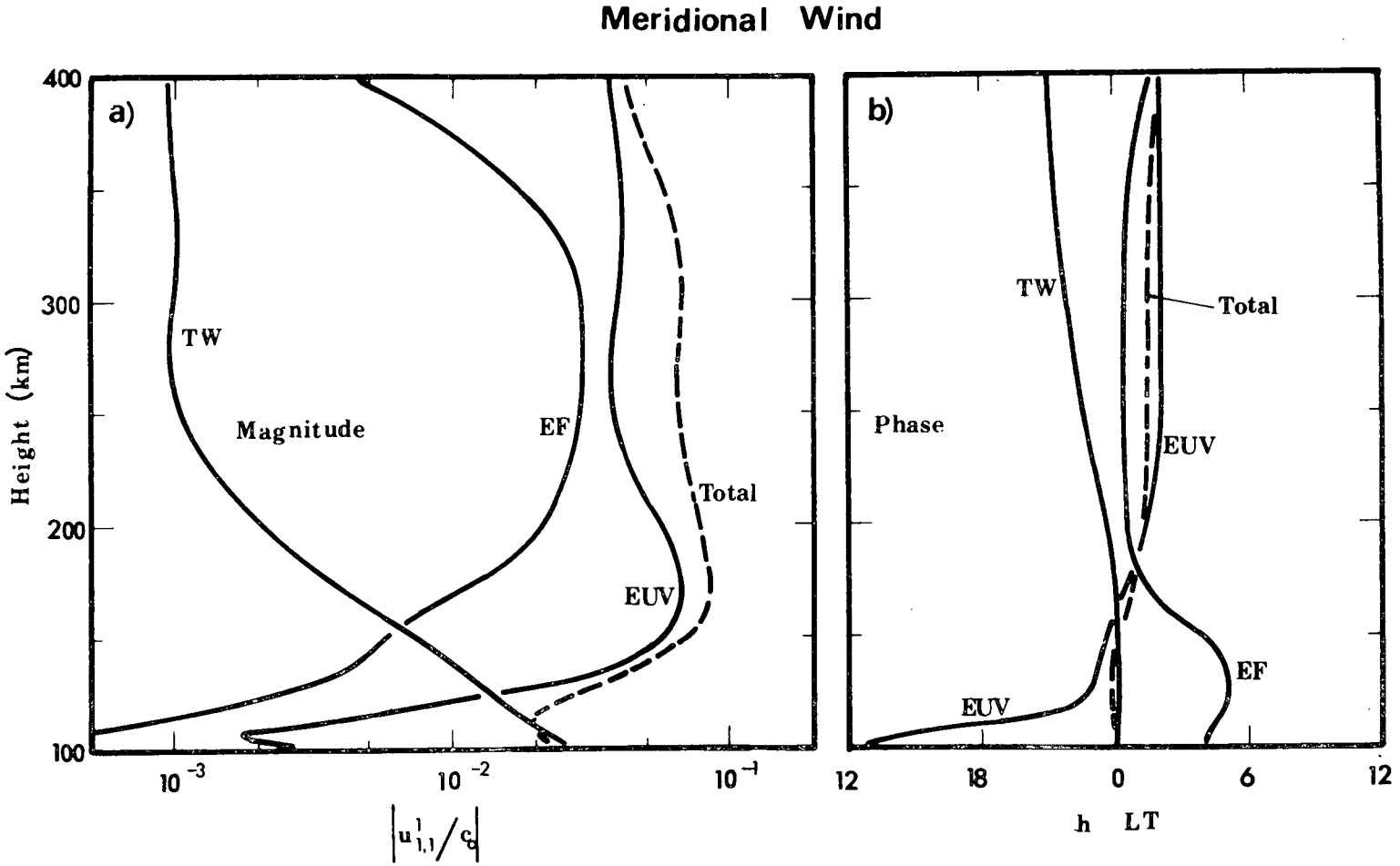

Figure 4. Magnitude (Fig. 4a) and phase (Fig. 4b) of the meridional wind coefficient $u^1_{1,1}/c_0$ of the diurnal (1, 1, 1)-mode versus altitude generated by the solar EUV heat input Q^1_{111} ("EUV") by the electric field of the Sq current ("EF") and by a heat source within the lower atmosphere ("TW"). The dashed lines give the sum of the three contributions.

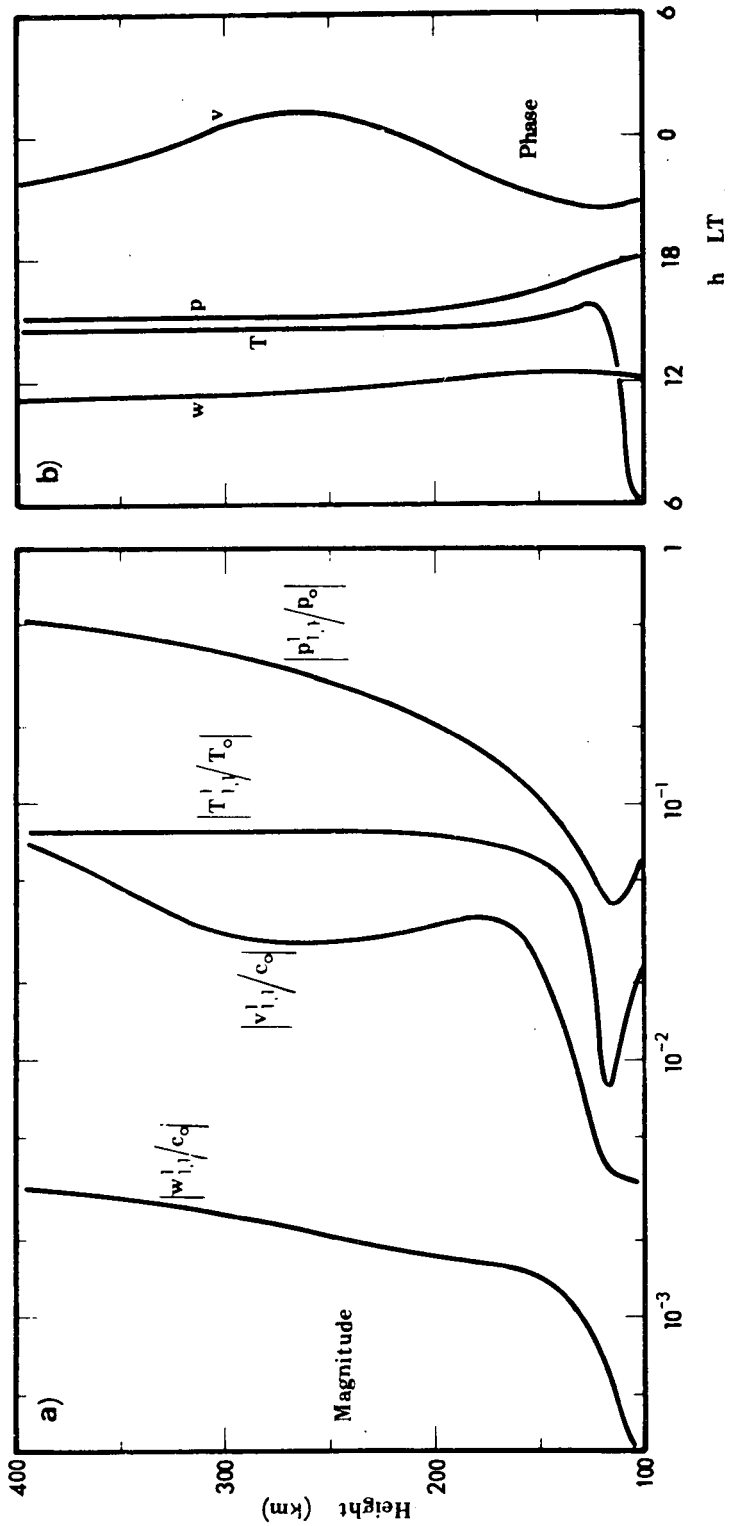

Figure 5. Magnitudes (Fig. 5a) and phases (Fig. 5b) of the coefficients of pressure $p^1_{1,1}/p_0$, temperature $T^1_{1,1}/T_0$, zonal wind $v^1_{1,1}/c_0$ and vertical wind $w^1_{1,1}/c_0$ of the diurnal (1, 1, 1)-mode versus altitudes generated by the sum of the three wave generators considered.

$v^1_{1,1}/c_0$ generated by the sum of EUV heat source III, electric field and wave from below. This figure shows a general behavior expected from the simplified theory in paper I. Pressure, vertical wind and zonal wind tend to increase with height to an asymptotic value. The temperature remains nearly constant above 200 km.

An interesting feature in Fig. 5a is the relative minimum of temperature and pressure near 120 km which is due to the steep mean vertical temperature gradient in this height range. The exact shape of the horizontal wind profiles above 300 km in Fig. 4a and 5a is subject the some ambiguity in our model because we introduced an effective collision number in order to simulate the influence of molecular viscosity. However any realistic change of this effective collision number above 300 km although altering somewhat the horizontal wind profile does not influence very much the temperature and pressure profile in Fig. 5a.

The times of maximum in Fig. 5b are nearly constant with altitude above 200 km indicating the quasi-evanescent nature of this wave mode at thermospheric altitudes.

Figure 6 gives the magnitudes of the coefficients a_3/a_2, a_4 and b_3/b_2 from Eq. (26) which are responsible for the latitude structure of pressure (and therefore temperature, density, and vertical wind) and zonal wind. The number a_4 which is identical with the coefficient $\delta_{1,3,1}$ in (7a) decreases from 0.3 at 100 km to a value of $|a_4| < 0.02$ above 250 km. Thus, the influence of the spherical harmonic $P_{3,1}$ in (19) decreases with height, so that above about 250 km only the spherical harmonic $P_{1,1}$ determines the latitude structure of the pressure. A similar situation exists for the zonal wind which is generated by EUV heat. Here the ratio $|v^1_{3,1}/v^1_{1,1}|$ decreases from a factor of four at 100 km to a value < 0.2 above 200 km altitude again diminishing the influence of the spherical function $P_{3,1}$ in (19), so that the zonal wind becomes nearly independent of latitude. However the significant amplitude of the zonal wind structure generated by the electric field is mainly determined by the ratio $|b_3/b_2|$ which remains nearly constant above 200 km.

In Fig. 7 we show the latitude structures of relative pressure p/p_0, meridional wind u and zonal wind v of tical mode (1,1,1) for four different heights. Here we notice again the degeneration of the pressure function from the Hough-function (1, -1) at 100 km to the spherical function $P_{1,1} = \sin\theta$ above 200 km altitude where it is identical with Jacchia's pressure bulge (Jacchia and Slowey, 1967). The meridional wind does not change its structure in our theory because of the assumptions made in (17). At 100 km the zonal wind becomes zero at 25° latitude and changes its sign there. This results from the influence of the spherical function $P_{3,1}$. The abrupt phase transition becomes more gradual

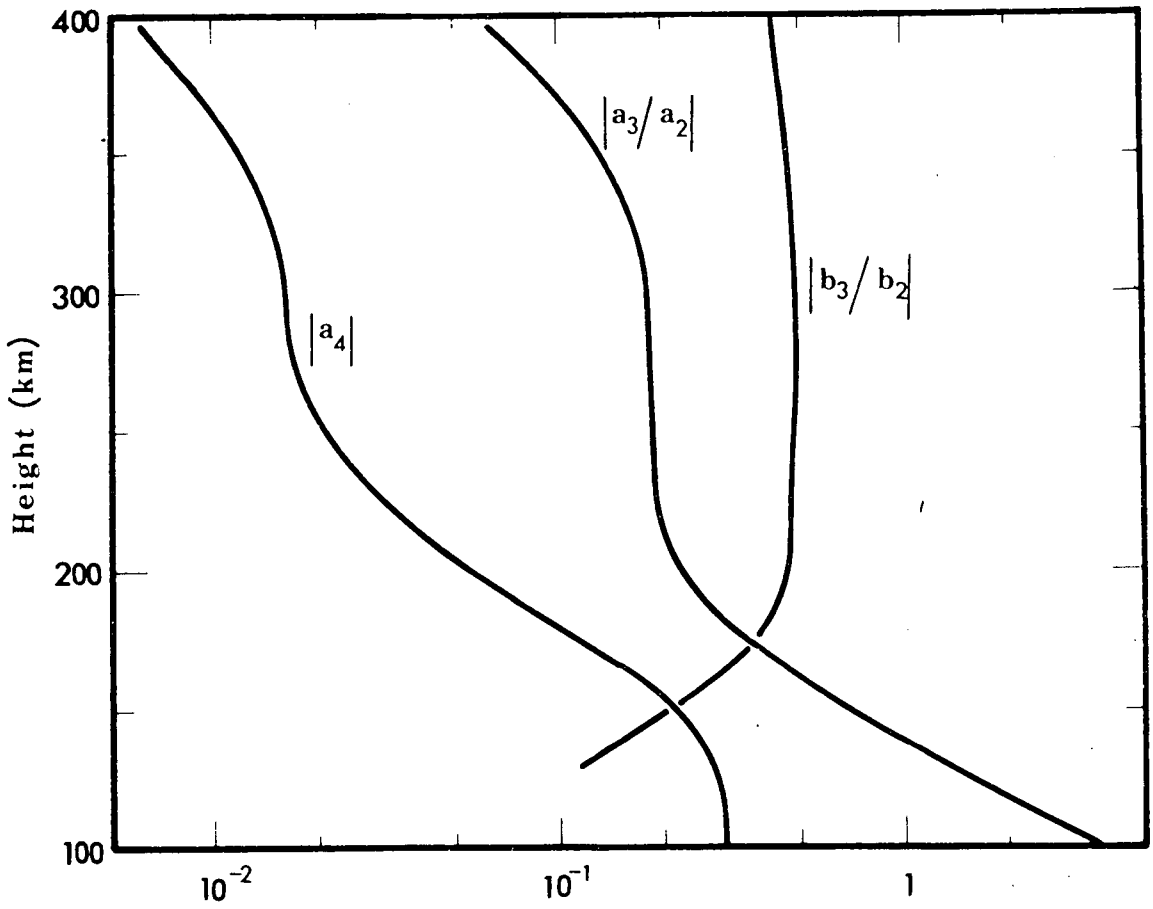

Figure 6. Height functions determining the latitude structures of pressure and zonal wind of the (1, 1, 1)-mode.

with increasing height although it is still evident at 300 km altitude. Since for the EUV induced wave the phase transition is already small above 300 km (see Fig. 6 and paper I), it is the electric field induced wave which is responsible for the phase change in Fig. 7c. The electric field induced wave essentially maps the zonal wind structure of the E-region into the F2 region.

The horizontal wind structure is plotted versus local time on the northern hemisphere in Fig. 8. In Fig. 8a the wind at 100 km is identical with the wind field of the tidal (1, -1) mode (Kato, 1966). The maximum northerly wind blows at 0^h local time at the poles. Moreover, we observe the reversal of the zonal wind direction at 25° latitude. In Fig. 8b we plotted the wind field of the EVU generated wave at 300 km altitude. Here the reversal of the zonal wind direction has disappeared, and the maximum northerly wind blows at 2.4^h at the poles. Fig. 8c finally gives the wind field at 300 km due to the sum of the EUV-heat,

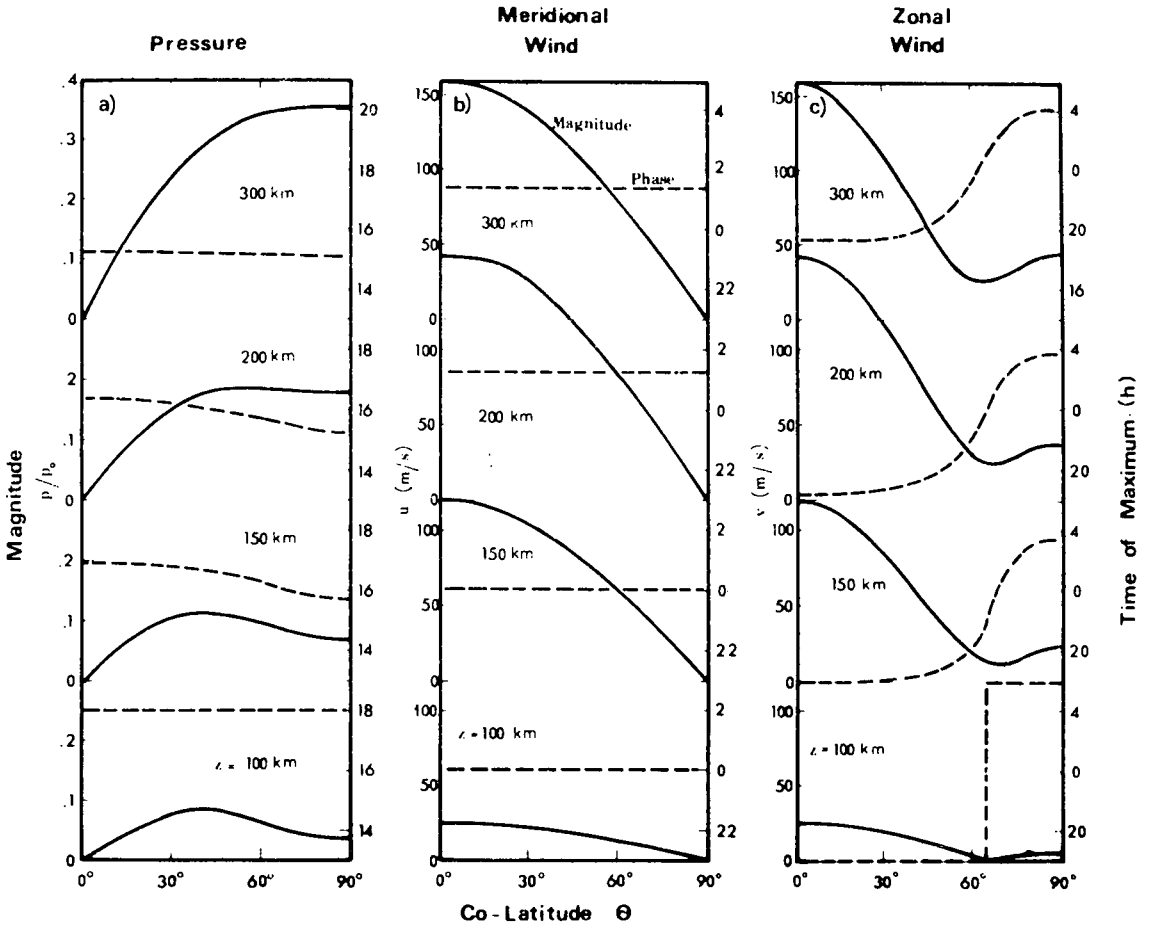

Figure 7. Total pressure, meridional wind and zonal wind versus colatitude θ of the diurnal (1, 1, 1)-mode calculated for four different heights. Solid lines: magnitudes; dashed lines: phases.

electric field and wave from below. Now a reversal of the zonal wind direction again exists near 30° latitude in the morning and the evening hours, and the maximum northerly wind has shifted to 1.2 hours local time. Besides this phase shift, both wind fields in Figs. 8b and 8c have similar structures apart from the morning and evening sectors at low latitudes.

Figure 8b is similar to the wind fields derived from the Jacchia model by Kohl and King (1967) and by Geisler (1967). (Note that we consider only the diurnal component whereas, in Jacchia's model a small but significant semidiurnal component is included). Kohl et al., (1968) have calculated from the ionospheric continuity equation diurnal variations of the critical F2 frequency and of the critical height for various stations. In these calculations the horizontal neutral

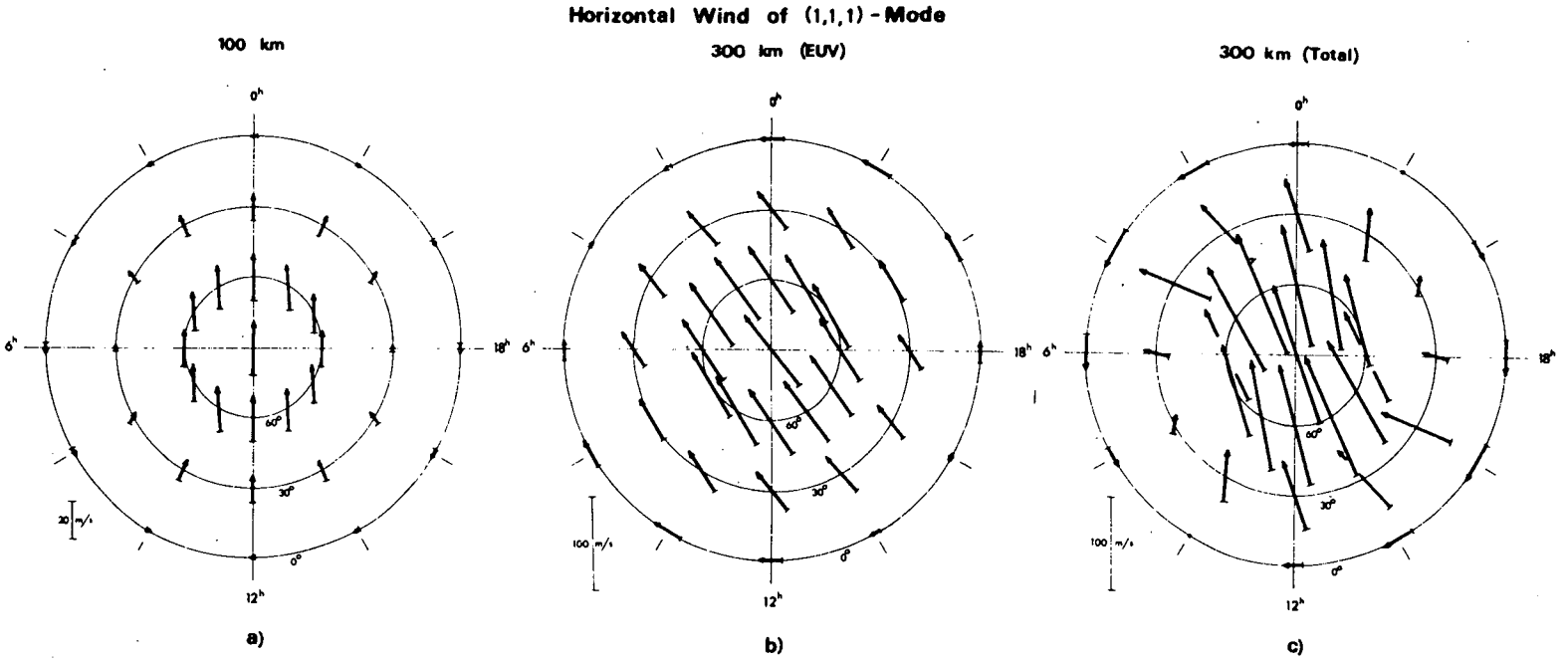

Figure 8a. Wind field at 100 km corresponding to the wind field of the Hough-function (1, -1) (Kato, 1966).

Figure 8b. Wind field at 300 km due to solar EUV heat input.

Figure 8c. Wind field at 300 km due to the sum of EUV heat input and the contribution from the electric field of the Sq current.

Figure 8. Horizontal wind field of the (1, 1, 1)-mode as function of local time on the northern hemisphere.

winds which cause vertical ionization drift have been adopted from the model of Kohl and King (1967). From a comparison between the experimental data and their theory, Kohl et al., (1968) concluded that a wind model with its phase advanced by 1.5 hours would improve the data fit very much. They already suggested electric fields as a possible cause for this shift. Our result in Fig. 8c verifies this suggestion. The electric field of the Sq current indeed prevents the phase of the F2 layer winds to shift by more than 1.2 hours with respect to the wind at E-layer heights.

8. THE FUNDAMENTAL SYMMETRIC SEMIDIURNAL TIDAL MODE (2,2,2)

In order to calculate the generation and propagation of the symmetric semidiurnal mode (2,2,2) we used the same model of the mean thermospheric properties and of ion drag as for the mode (1,1,1) in section 7. We furthermore adopted heat source Q_{III} in (31). However we reduced the total heat input of this source by a factor of 5/32 to $\bar{E}_{III} = 0.52$ erg/cm^2 sec. The factor 5/32 corresponds roughly to the ratio between the semidiurnal and the diurnal heat input components in a development into spherical functions (see paper I, Eq. (I/9)). Because of the apparaently small semidiurnal component of the tidal winds which generate the geomagnetic Sq current (Kato, 1956; Stening, 1969; Tarpley, 1970) we expect small effective electric polarization fields of this period at F2 layer heights. However, a solar semidiurnal gravitational potential of

$$\Phi = -3.7 \times 10^{-7} P_{2,2} \cos 2\tau \ (\mathrm{km}^2/\mathrm{sec}^2) \tag{34}$$

(Siebert, 1961) acts like an additional driving mechanism for such a wave. In the case of the nondissipative lower atmosphere it can be shown (see paper I Eq. (II/34)) that the gravitational driving force in (11c) becomes

$$\left|(F\,g)^2_{2,2}\right| \sim \left|\frac{35}{6\,\Omega^2\,r^2}\,\Phi^2_{2,2}\right| \sim 10^{-5} \tag{35}$$

where $\Phi^2_{2,2}$ is the coefficient of Φ in a development into a series of the Hough-functions. The number in (35) must be compared with the corresponding heat generator in (11c) which is

$$J^2_{2,2} \sim 0.005 \times \frac{5}{32} \sim 10^{-3}$$

at stratospheric altitudes. At thermospheric heights it is according to paper I, Eq. (II/26)

$$|(F\,g)^2_{2,2}| \sim \left| \frac{6\,\Phi^2_{2,2}}{f_k\,\Omega^2\,r^2} \right| \sim 2 \times 10^{-6}$$

while $J^2_{2,2} \sim 3 \times 10^{-3}$ there (see (33)). Therefore the tidal gravitational force does not significantly contribute to the semidiurnal solar tides at thermospheric heights.

However, the non-linear coupling from the tidal (1,1,1)-mode into the (2,2,2)-component via the diurnal term $\nu_{1,1}$ of the collision number (see Eqs. (2) and (21)) may give rise to significant amplitudes. The coefficients $A^2_{r,1}$ and $B^2_{r,1}$ in (21) have been calculated according to the scheme given in (22), and the wind coefficients $u^1_{1,1}$ and $v^1_{1,1}$ from Figs. 4 and 5 have been adopted in order to determine a virtual external force in (10) or (11c) which acts like the generator of semidiurnal waves in addition to the EUV-solar heat input.

Finally we added to these two wave generators a wave generator situated within the lower atmosphere below 100 km. According to the few direct observations at E-layer heights (Greenhow and Neufeld, 1961; Rosenberg and Edwards, 1964; Roper and Elford, 1965; Zimmermann and Marcos, 1967; Murphy and Bull, 1968; Bernard, 1971) the tidal (2,4,2) component seems to dominate at E-layer heights with wind amplitudes of the order of 10m/sec. This wave has disappeared above 200 km altitude which can readily be explained by the filtering effect of the thermosphere dynamic system (see paper I, Eq. (I/49)). At higher altitudes the (2,2,2) component is the dominant semidiurnal component (see paper I, Eq. (I/14)). Due to our ignorance about the semidiurnal (2,2,2) component at E-layer heights we can do only sample calculations of the wave from below such that the numerical results are consistent with the observations above 200 km. For this reason we selected a density amplitude at 100 km for the wave from below of $\rho^2_{2,2}/\rho_0 = 0.008$ peaking at 2.7 hours local time. These two numbers are not completely arbitrary because they correspond to a heat input of $J^2_{2,2} = 1.4 \times 10^{-3}$ with maximum heat at 0 hour local time within the height region between 70 and 100 km where this wave is a trapped wave. This is equivalent to a solar heat input proportional to cos x (x is the zenith distance) into this height range with maximum amplitude of J = 0.004 at 12 hour local time.

Figure 9a shows the relative density amplitude versus height generated by the three wave generators considered as well as the sum of the three contributions (dashed line). The (2,2,2)-mode being a trapped mode between 70 and 100 km becomes a propagation mode above 100 km altitude. Therefore between 100 and 120 km we notice in Fig. 9a a nearly exponential increase of the tidal wave from below (Symbol "TW"). Above 120 km however, this increase is compensated by the dissipative effects of heat conduction and ion drag transforming the (2,2,2)-mode into a quasi-trapped mode with nearly constant amplitude with height. The behavior of the EUV-generated wave (Symbol "EUV") is quite normal and similar to that of the diurnal mode in Fig. 3a with the difference that its amplitude is already more pronounced below 200 km due to the propagation characteristics of this semidiurnal mode within the lower thermosphere. The drag induced component (Symbol "DR") which resulted from the non-linear coupling between the diurnal and semidiurnal mode is unimportant below 250 km. However, it becomes a significant fraction of the total wave above this height. The wave from below dominates below 200 km and is still non-negligible above this height.

Figure 10a gives the relative temperature amplitudes versus height of the three components with a similar behavior as in Fig. 9a apart from the fact that the wave from below ceases to dominate already above 160 km. The maximum times of density and temperature are given in Figs. 9b and 10b. The EUV-generated wave peaks near 1h L.T. above 200 km altitude while the drag induced components peak near 3h L.T. The density amplitude of the wave from below changes its phase with height from 2.7h at 100 km to 7.4h at 400 km. The temperature amplitude of the wave from below is phase advanced by about 3 hours with respect to the density. This phase advance causes a time delay of 1 to 4 hours between temperature and density of the total wave (the dashed lines) between 200 and 300 km. This time delay in the semidiurnal component is consistent with the results from a Fourier analysis of the observed neutral density and ion temperature (Volland, 1970) and contributes to explain the difference between the times for the density and temperature maxima.

At 400 km height the ratio between semidiurnal and diurnal density is according to Figs. 3a and 9a

$$|\rho^2_{2,2}/\rho^1_{1,1}| \sim 0.08.$$

This number agrees well with the corresponding number from the Jacchia-model (Jacchia and Slowey, 1967) which is (see paper I, Eq. (I/14))

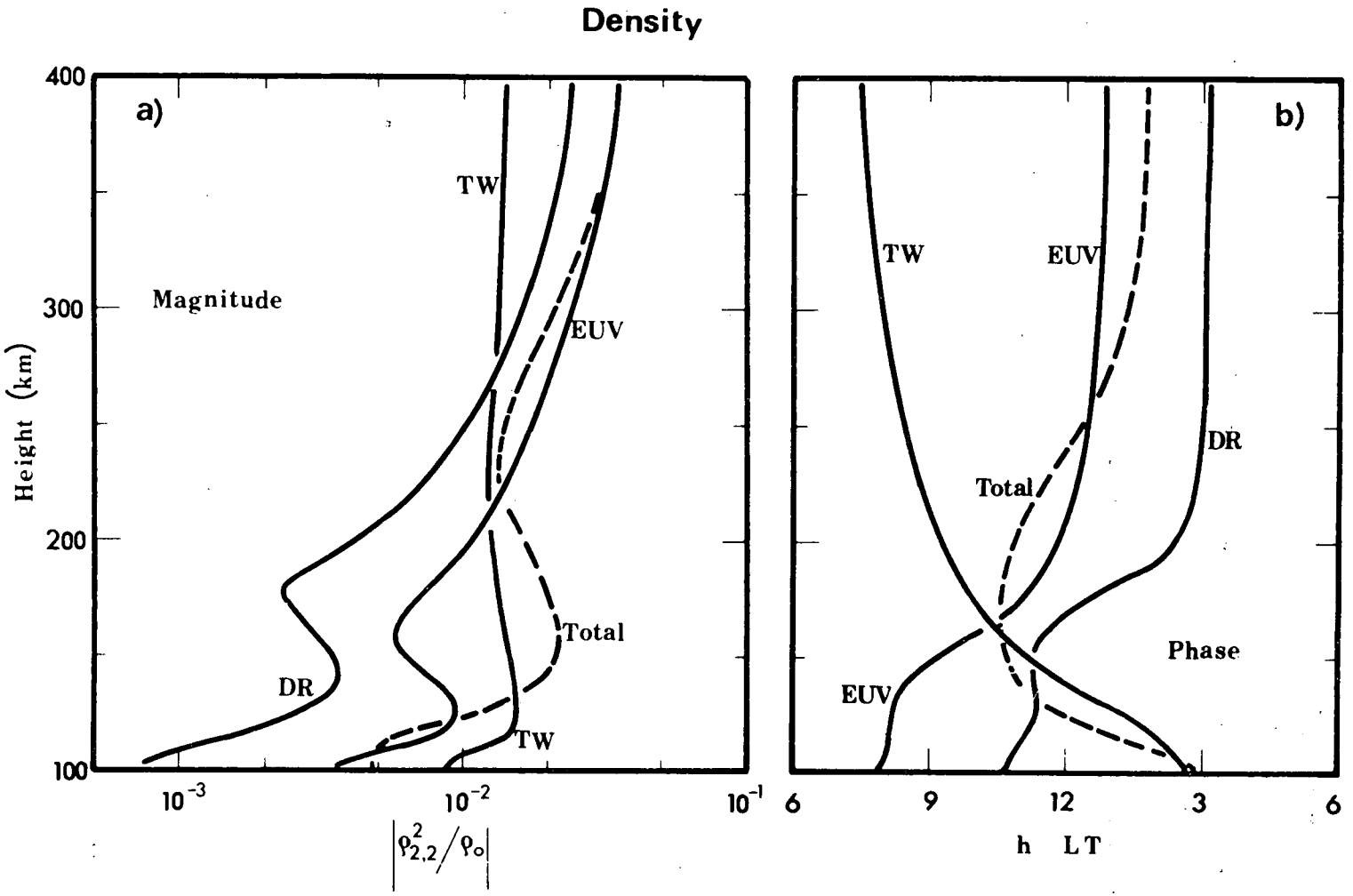

Figure 9. Magnitude (Fig. 9a) and phase (Fig. 9b) of the density coefficient $\rho^2_{2,2}/\rho_0$ of the semidiurnal (2, 2, 2)-mode versus altitude generated by the solar EUV heat input ("EUV"), by drag induced coupling ("DR") and by a heat source within the lower atmosphere ("TW"). The dashed lines give the sum of the three contributions.

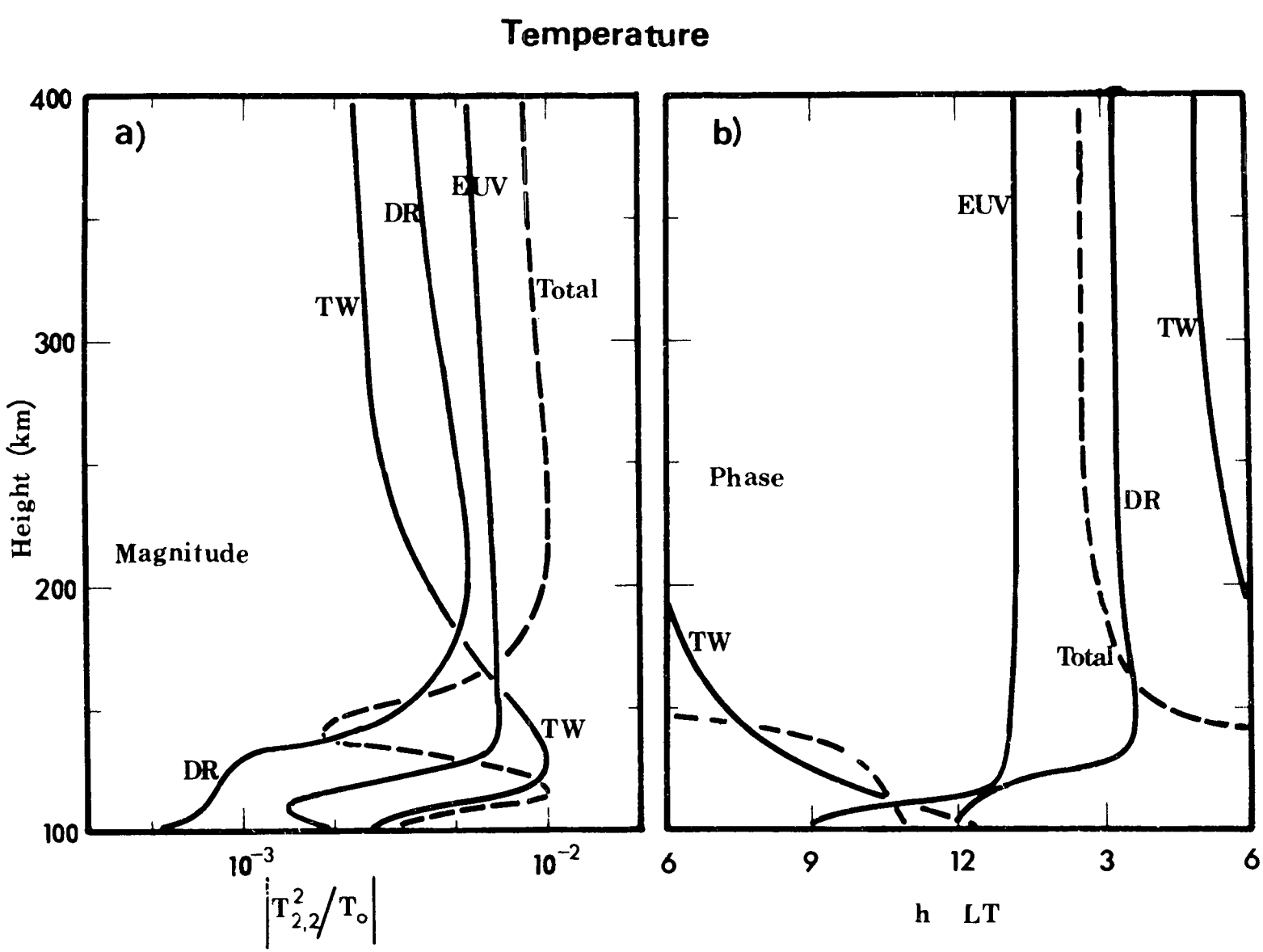

Figure 10. Magnitude (Fig. 10a) and phase (Fig. 10b) of the temperature coefficient $T^2_{2,2}/T_0$ of the semidiurnal (2, 2, 2)-mode versus altitude generated by the solar EUV heat input ("EUV"), by drag induced coupling ("DR") and by a heat source within the lower atmosphere ("TW"). The dashed lines give the sum of the three contributions.

$$|T_{2,2}/T_{1,1}| \sim \frac{0.035}{0.12\sqrt{12}} = 0.084$$

(Note that Jacchia's exospheric temperature is merely a measure of the observed density).

Figure 11 shows the coefficients of horizontal winds, vertical wind and pressure generated by the sum of the three wave generators considered. Since the drag induced fraction of the horizontal winds exceeds the EUV-induced winds between 200 and 300 km and since the phases of both components differ by about 6 hours the amplitudes and phases of the total horizontal winds are rather variable with height. Above 300 km this may not be realiatic because of our simplifying assumption about viscosity. However pressure and vertical wind behave in a normal manner. An important feature in Fig. 11b is the strong phase change with height of the horizontal winds which covers about 2/3 of a period between 100 and 300 km.

It is this phase transition which prevents the semidiurnal mode from generating a significant contribution to the geomagnetic Sq current (Tarpley, 1970).

Figure 12 finally shows the change with altitude of the latitude structure of relative pressure, meridional wind and zonal wind of the semidiurnal (2,2,2)-mode. Here again we notice the transition of the pressure structure from the Hough-function (2,2) at 100 km to the spherical function $P_{2,2}$ above 200 km (see paper I). Moreover the horizontal winds having magnitudes smaller than 5m/sec at 100 km reach amplitudes of 45m/sec at 150 km and then decrease again to the order of 10m/sec above 200 km altitude. This wind field must be added to the wind structure of the diurnal (1,1,1)-mode in Fig. 7 or 8. It may significantly influence the total horizontal wind structure between 100 and 200 km especially at low and medium latitudes.

CONCLUSION

We did a numerical calculation of the generation and propagation of two important symmetric tidal waves within a realistic thermosphere model. These fundamental modes are the diurnal wave (1,1,1) which is described by the Hough function (1,-1) at lower altitudes and which degenerates into the spherical function $P_{2,2}$ at thermospheric altitudes, and the fundamental semidiurnal mode (2,2,2) which is described by the Hough function (2,2) within the lower non dissipative atmosphere and which degenerates into the spherical function $P_{2,2}$ at thermospheric altitudes. Both wave modes are predominantly generated by the solar EUV heat input into the thermosphere. In the case of wave mode (1,1,1),

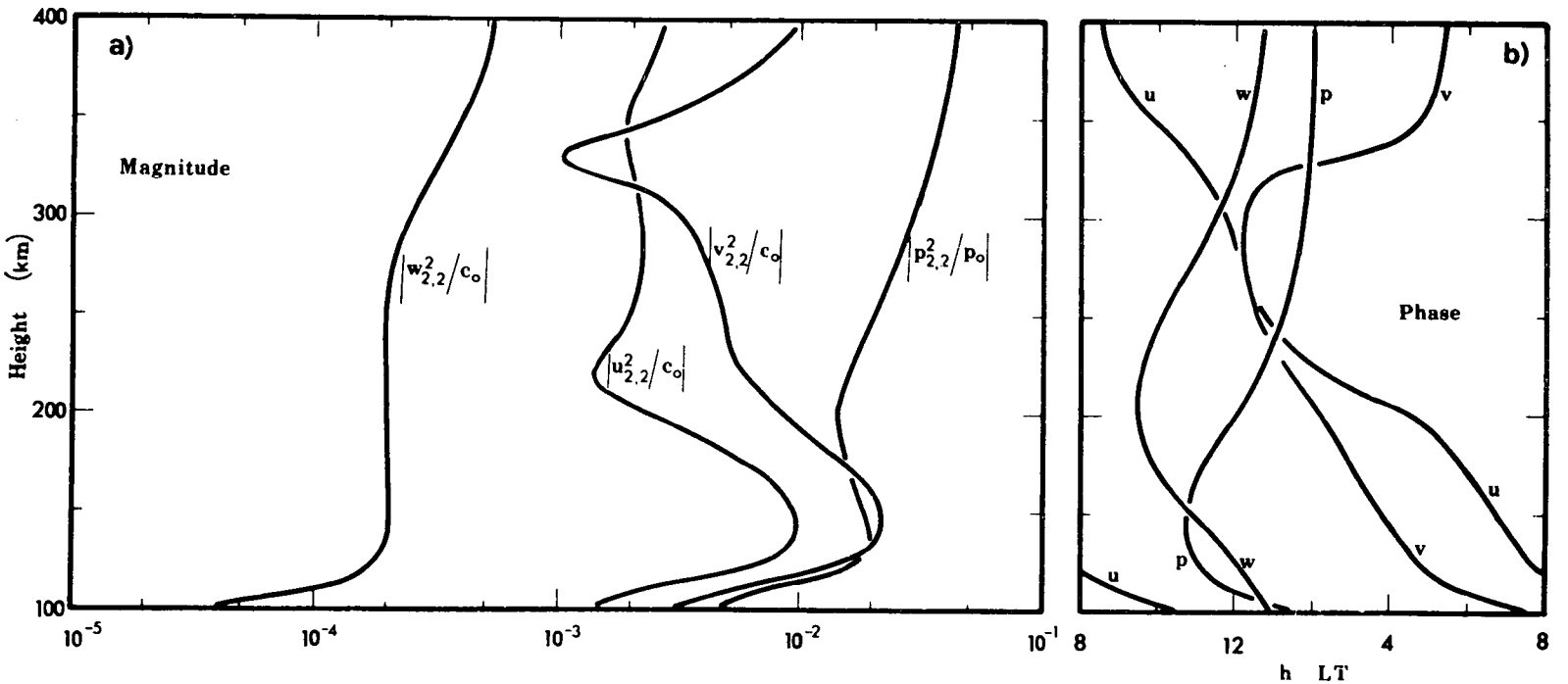

Figure 11. Magnitudes (Fig. 11a) and phases (Fig. 11b) of the coefficients of pressure $p^2_{2,2}/p_0$, meridional wind $u^2_{2,2}/c_0$, zonal wind $v^2_{2,2}/c_0$ and vertical wind $w^2_{2,2}/c_0$ of the semidiurnal (2, 2, 2)-mode versus altitude generated by the sum of the three wave generators considered.

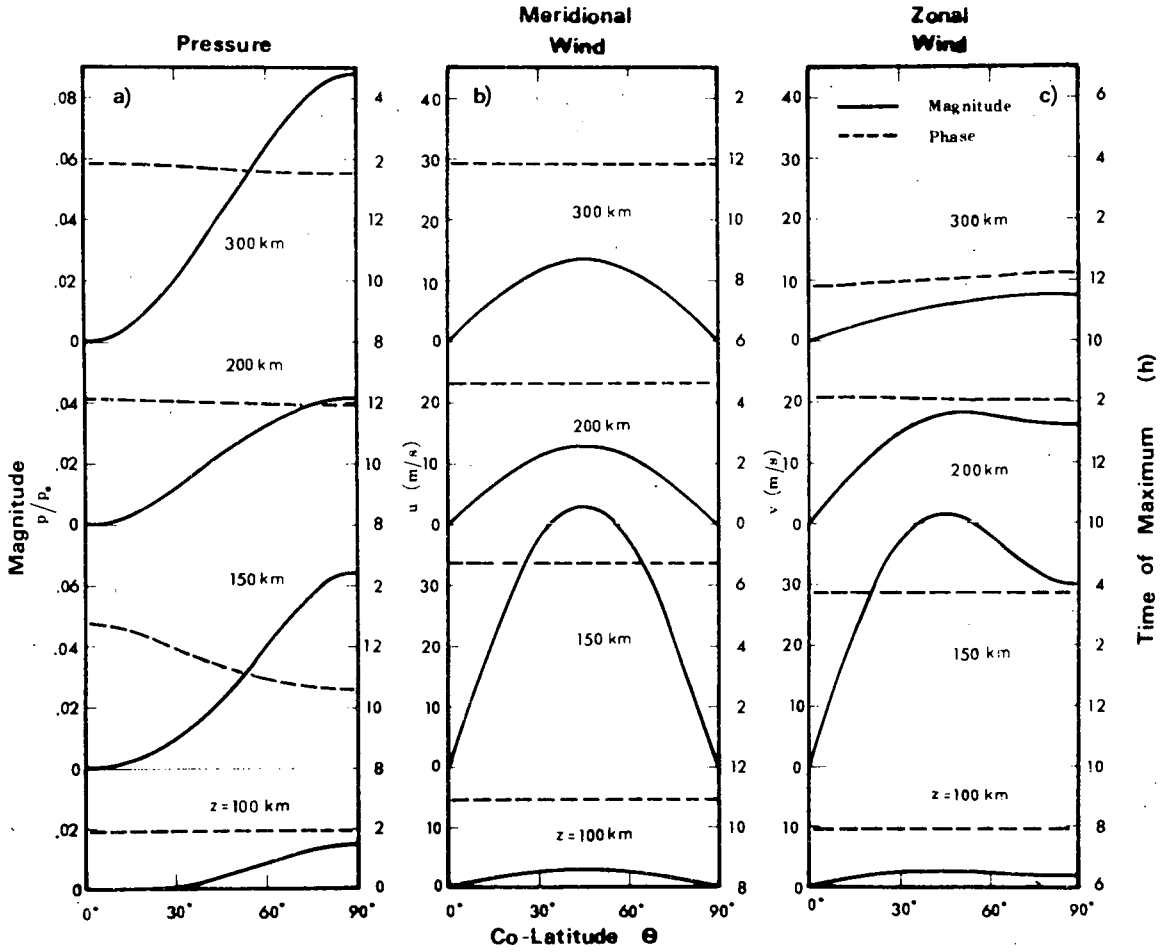

Figure 12. Total pressure, meridional wind and zonal wind versus colatitude θ of the semidiumal (2, 2, 2)-mode calculated for four different heights. Solid lines: magnitudes; dashed lines: phases.

the contribution of the wave which is generated below 100 km decays rapidly with height and becomes insignificant above 180 km. The electric polarization field of the geomagnetic Sq current which maps into the upper part of the thermosphere generates via ion-neutral drag a significant fraction of the wind components of this wave mode at F2 layer heights. The latitude structure of this mode constitutes the pressure bulge of the neutral air at thermospheric heights the diurnal component of which peaks at 15h L.T. (Jacchia and Slowey, 1967). The horizontal wind field of the EUV-generated wave above 200 km is nearly identical with the wind system derived by Geisler (1967) and by Kohl and King (1967). The electric field induced wind component shift the phase of the total wind by about 1 hour to earlier times at 300 km altitude. This phase advance was expected from a study of the influence of neutral air winds on the ionospheric F2 layer (Kohl et al., 1968).

In the case of the semidiurnal mode (2,2,2), electric polarization fields of E-layer origin as well as the solar semidiurnal gravitational tidal force appear to be negligibly small. However, the wave component generated below 100 km can penetrate deep into the thermosphere and remains significant even at 400 km altitude. Moreover non-linear momentum coupling from the (1,1,1)-mode into the (2,2,2)-mode due to the diurnal variation of the ion-neutral collision number becomes important at F layer heights. The wave from below propagating as free internal wave at thermospheric heights has a phase delay between its density and temperature amplitudes of about 3 hours while density and temperature of the EUV-induced wave component peak both at about the same time at 13h L.T. Due to the interference between the wave from below, the EUV-induced component and the drag induced component the temperature amplitude of the total semidiurnal wave peaks at about 15h L.T. whereas the density has its maximum at 13h L.T. at F layer heights. This phase delay between temperature and density of the semidiurnal mode contributes to the difference between the times of maximum of the neutral thermospheric density (determined from satellite drag data) and the neutral thermospheric temperature (determined from Thomson scattering measurements).

REFERENCES

Bernard, R.	1971	Semidiurnal tide in the E-region observed by incoherent scatter measurements above Saint Santin, Space Res. XII (to be published)
Chapman, S. Lindzen, R. S.	1970	Atmospheric tides. D. Reidel Publ. Comp., Dordrecht, Holland
Geisler, J. E.	1967	A numerical study of the wind system in the middle thermosphere. J. Atm. Terr. Phys. 29, 1469 - 1482
Greenhow, J. S. Neufeld, E. L.	1961	Winds in the upper atmosphere. Quart. Journ. Roy. Meteorol. Soc. 87, 564-574
Hays, P. B.	1970	Composition and heating of the thermosphere. EOS, 51, 787
Hinteregger, H. E. Hall, L. A. Schmidtke, G.	1965	Solar XUV radiation and neutral particle distribution in July 1963 thermosphere. Space Res. V, pp. 1175-1190
Jacchia, L. G.	1965	Static diffusion models of the upper atmosphere with empirical temperature profiles. Smithsonian Contr. Astrophys. 8, 215-257
Jacchia, L. G. Slowey, J.	1967	The shape and location of the diurnal bulge in the upper atmosphere. Space Res. VII, pp. 1077-1090
Kato, S.	1956	Horizontal wind systems in the ionospheric E-region deduced from the dynamo theory of the geomagnetic S_q variation. Part II: Rotating earth, Journ. Geomagn. Geoelectr. 8, 24-37
Kato, S.	1966	Diurnal atmospheric oscillations. Journ. Geophys. Res. 71, 3201-3214
Kato, S. Matsushita, S.	1969	A consideration on the tidal wave transmission through the ionized atmosphere. Journ. Geomagn. Geoelectr. 21, 471-478

King-Hele, D. G. Hingston, J.	1967	Variation in air density at heights near 150 km from the orbit of the satellite 1966-101J, Planet. Space Sci. 15, 1883-1893
King-Hele, D. G. Hingston, J.	1968	Air density at heights near 190 km from the orbit of SECOR 6, Planet. Space Sci. 16, 675-691
Kohl, H. King, J. W.	1967	Atmospheric winds between 100 and 700 km and their effect on the ionosphere. Journ. Atm. Terr. Phys. 29, 1045-1062
Kohl, H. King, J. W. Eccles, D.	1968	Some effects of neutral air winds on the ionospheric F-layer. Journ. Atm. Terr. Phys. 30, 1733-1744
Murphy, C. H. Bull, G. V.	1968	Ionospheric winds over Yuma, Arizona, measured by gun-launched projectiles. Journ. Geophys. Res. 73, 3005-3015
Obayashi, T.	1964	The electric state of the upper atmosphere. Journ. Geomagn. Geoelectr. 15, 133-147
Pitteway, M. L. V. Hines, C. O.	1963	The viscous damping of atmospheric gravity waves, Can. J. Phys. 41, 1935-1948
Roper, R. G. Elford, W. G.	1965	Periodic wind components at meteor heights. Document X-650-65-86, NASA Goddard Space Flight Center, Greenbelt/Md., USA
Rosenberg, N. W. Edwards, H. D.	1964	Observations of ionospheric wind patterns through the night. Journ. Geophys. Res. 69, 2819-2826
Siebert, M.	1961	Atmospheric tides. Adv. Geophysic 7, 105-187
Spencer, N. W. Taeusch, D. R. Carignan, G. R.	1966	N_2 temperature and density data from the 150 to 2300 km region and their implications Ann. Geophys. 22
Stening, R. J.	1969	An assessment of the contributions of various tidal winds to the Sq current system. Planet. Space Sci. 17, 889-908

Taeusch, D. R. Niemann, H. B. Carignan, G. R. Smith, R. E. Balance, J. O.	1968	Diurnal survey of the thermosphere. I: Neutral partical results. Space Research VIII, p. 930-939, North Holland Publishing Company, Amsterdam
Tarpley, J. D.	1970	The ionospheric wind dynamo, Part II, Planet. Space Sci. 18, 1091-1103
Volland, H.	1970	Phase delay between neutral temperature and neutral density at thermospheric heights Journ. Geophys. Res. 75, 5618-5620
Volland, H.	1971	A simplified model of the geomagnetic Sq current system and the electric fields within the ionosphere. Cosmical Electrodyn. 1, 428-459
Volland, H. Mayr, H. G.	1970	A theory of the diurnal variations of the thermosphere. Ann. Geophys. 26, 907-919
Volland, H. Mayr, H. G.	1971	A three dimensional model of thermosphere dynamics. NASA-Document X-621-71-240/241/242, GSFC, Greenbelt/Md., USA
Zimmermann, S. P. Marcos, F. A.	1967	Measurements of tidal oscillations above 120 km, AF CRL-67-0131, Environmental Research Papers, No. 266, Office of Aerospace Research, Bedford, Mass.